KERNFORSCHUNGSZENTRUM

KARLSRUHE

Dezember 1974

KFK 2087

Institut für Angewandte Kernphysik

Deformation of ^{56}Fe from 104 MeV α-Particle Scattering

H.J. Gils, H. Rebel, G. Nowicki, D. Hartmann,
(Kernforschungszentrum Karlsruhe)
A. Ciocănel
(Atomic Physics Institute, Bucharest, Romania)
H. Klewe-Nebenius, K. Wisshak
(II. Physikalisches Institut der Universität Heidelberg)

GESELLSCHAFT
FÜR
KERNFORSCHUNG M.B.H.

KARLSRUHE

GESELLSCHAFT FÜR KERNFORSCHUNG M.B.H.

KARLSRUHE

KERNFORSCHUNGSZENTRUM KARLSRUHE

KFK 2087

Institut für Angewandte Kernphysik

Deformation of ^{56}Fe from 104 MeV α-Particle Scattering

von

H.J. Gils, H. Rebel, G. Nowicki, A. Ciocănel[+]
D. Hartmann, H. Klewe-Nebenius[++] and K. Wisshak[++]

[+] Permanent address: Atomic Physics Institute, Bucharest Romania

[++] II. Physikalisches Institut der Universität Heidelberg

Gesellschaft für Kernforschung m.b.H., Karlsruhe

Abstract

Differential cross sections have been measured for the elastic and inelastic scattering of 104 MeV α-particles from ^{56}Fe. The angular distributions are analyzed in terms of coupled channels on the basis of a symmetric and asymmetric rotator model. The analyses use a semimicroscopic folding procedure /1/ and additionally in some cases the conventional extended optical model. Deformation parameters, rms-radii, multipole moments of nuclear matter, and transition probabilities have been extracted.

Untersuchung der Deformation von ^{56}Fe mit 104 MeV α-Teilchen Streuung

Zusammenfassung

Am Karlsruher Isochronzyklotron wurden differentielle Wirkungsquerschnitte der elastischen und inelastischen Streuung von 104 MeV α-Teilchen an ^{56}Fe gemessen. Die experimentellen Daten wurden durch "coupled-channel" Rechnungen auf der Basis eines symmetrischen und eines dreiachsial-asymmetrischen Rotationsmodells analysiert. Dabei wurde ein halbmikroskopisches Faltungsverfahren benutzt, das eine deformierte Nukleonendichteverteilung zugrunde legt. Es werden mittlere quadratische Radien und innere Multipolmomente der Nukleonenverteilung berechnet und Übergangswahrscheinlichkeiten angegeben.

1. Introduction

Level schemes and E2-properties of nuclei in the 1f-2p-shell indicate collective features intermediate between harmonic vibrations and rigid rotations (cf Lesser et al. 1972, Towsley et al. 1972, Parikh 1972, Chandra and Rustgi 1972, Rebel et al. 1972a, 1973a, 1973b). The magnitude of B(E2)-values and the static quadrupole moments Q_{2^+} of the first excited 2^+ states provide a sensitive measure for the deformation of the nuclear surface. According to the usual rotational model, the sign of Q_{2^+} distinguishes between prolate and oblate shape of the nucleus. Electromagnetic transition probabilities and static quadrupole moments have been measured by nuclear resonance fluorescence (Kelly and Beard 1961, Metzger 1961) and Coulomb excitation experiments (Andreyev et al. 1960, Lesser et al. 1972, Towsley et al. 1972), respectively. In particular the large quadrupole moment and the E2-properties of ^{56}Fe exhibit this nucleus to be a strongly deformed almost pure prolate rotator. The experimental B(E2; $0^+ \rightarrow 2^+$), B(E2; $2^+ \rightarrow 4^+$) and Q_{2^+} values correspond to intrinsic quadrupole moments Q_o of 93 $\pm$ 8 (Metzger 1961), 98 $\pm$ 1, 99 $\pm$ 20 and +87 $\pm$ 20 e fm^2 (Lesser et al. 1972), derived on the basis of a symmetric rotator. Assuming a triaxial asymmetric nucleus with an asymmetry angle $\gamma = 20^o$ the measured probabilities are also consistent with Q_o = 102 e fm^2. Davydov and Chaban (1960) explained the level scheme of ^{56}Fe in the framework of an asymmetric rotator model with ß-vibrations resulting in $\gamma = 17^o$ and a softness parameter $\mu = 0.61$. Recently, an analysis (Rebel et al. 1974) of the level scheme and B(E2)-values of ^{56}Fe was performed on the basis of the

---

Zum Druck eingereicht am 15.11.1974

generalized collective model worked out by Gneuss and Greiner (cf Gneuss and Greiner 1971, Gneuss et al. 1969, 1970). The resulting collective energy surface representing the potential energy $V(\beta,\gamma)$ in an intrinsic frame and in terms of the usual shape parameters β and γ shows two minima in the range of the zero-point oscillation: one potential energy minimum for a prolate shape, the other representing an asymmetrically deformed shape.

In this paper, we report investigations of the collective behavior of ^{56}Fe which use the scattering of 104 MeV α-particles. First results of this experiment have been already published elsewhere (Gils et al. 1974a). The experiment aimed at specific information on the shape and intrinsic mass quadrupole moment of the ^{56}Fe nucleus. Because of the strong absorption in nuclear matter medium energy α-particle scattering is a surface reaction and therefore an excellent tool for the study of nuclear deformations. Previous studies of the elastic and inelastic α-particle scattering (Rebel et al. 1972a, 1973b) have shown that these experiments are not only sensitive to higher order deformations such as hexadecapole components in nuclear shape but also sensitive to the sign of the deformation parameters (Rebel 1972). This is due to the interference of single- and higher-order excitation processes which influence the observed distinct diffraction patterns of the differential cross sections and which allow discrimination between prolate and oblate nuclear shapes by a coupled channel analysis.

For 104 MeV α-particles the target-projectile interaction is mainly the nuclear interaction, which is conventionally parametrized as an optical potential. Though very successful in describing the scattering cross sections such a scattering model introduces an unavoidable model dependence into the extracted information. Furthermore, the relation between spatial size and deformation of the optical potential on the one side and of the nuclear matter density distribution on the other side is not quite clear and of complex nature. However, there is considerable evidence (Rebel 1974) that a simple procedure generating the real part of the optical potential by folding the projectile-bound nucleon interaction over the nucleon distribution provides an adequate way to relate size and shape of the nucleus to the experimental cross sections, at least in the diffraction region. The results for the rms-radius $\langle r^2 \rangle^{1/2}$ and for the intrinsic quadrupole moment Q_o quoted in this paper are extracted by such a folding model analysis of the experimental data.

2. Experimental procedure and results

The present (α,α') scattering experiments continue similar studies (Rebel et al. 1972a, 1973b) of the stable even Ni- and Ti-isotopes. The measurements used the scattering facilities at the 104 MeV α-particle beam of the Karlsruhe Isochronous Cyclotron. The target was a self supporting ^{56}Fe foil (99.5 % enrichement) of 2.1 ± 0.1 mg/cm^2 thickness. In a first run the α-particle beam was not energy-analyzed in order to avoid background from slit scattering and to extend the measurements of the elastic and 2_1^+ inelastic cross sections on to very forward angles (≈ 6^o lab). For a further independent run the α-particle beam was energy-analyzed to about 60 keV. The relatively large scattering chamber (130 cm diameter), a small beam spot (~ 1 mm width, ~ 2 mm height) and a beam divergence of about $\pm 0.1^{\circ}$ enabled a good angular accuracy ($\Delta\theta$(FWHM) $\approx 0.25^{\circ}$) of the angular distributions. The absolute zero of the angular scale has been determined by measuring the sharp diffraction minima on both sides of the incident beam. Beam currents were varied from a few nA to the order of 200 nA. The scattered α-particles were detected by four telescopes of two 2 mm transmission mounted silicon surface barrier detectors. The four telescopes were rigidly mounted to the same movable arm, with a fixed angle of 1.5° between them.

The set-up of the electronics is shown in fig. 1. It consists of a conventional pre- and main-amplifying system for each detector branch. The biased amplifiers select and stretch a small energy interval between 0 and about 5 MeV excitation energy out of the whole α-particle spectrum. The router unit sets additional bits - characterizing the origin of the converted pulse - to the on-line computer. The computer is programmed as a multichannel pulse height analyzer, and it stores the events in four 1K-memories one for each detector. The overall energy resolution was about 120-200 keV FWHM.

Particle identification was found not to be neccessary because the maximum energy loss of protons, deuterons, tritons and ^{3}He particles in 4 mm silicon is 26, 37, 43 and 93 MeV, respectively. So the (Z=1)-particles can only cause pulses in a region of the spectrum which is cut off by the biased amplifier. Due to the large difference in binding energies between ^{3}He and ^{4}He the maximum energy of ^{3}He particles produced is considerably lower than that of the elastically scattered α-particles.

Accidental coincidences between two or more detectors which may cause a wrong pulse height in the ADC were found to be negligible at the beam currents used. Therefore, it was not neccessary to use a special set-up of the routing unit which could suppress such pile-up events but which is more difficult to handle and to adjust. The measurements at very forward scattering angles were carried out with one detector only. More details of the experimental arrangement and the data handling have been described in previous papers (Rebel et al. 1973b, 1972a,b).

As an example fig. 2 shows an energy spectrum of the outgoing α-particles. For forward angles there are also contamination peaks from ^{12}C and ^{16}O which walk out of the region of interest (up to about 2.7 MeV) beyond 25°. In a detailed analysis of the energy spectra the continuous background was subtracted and the line shapes were fitted by an asymmetric Gaussian form thus separating in most cases the contribution of interfering contamination peaks. In fig. 2 the dashed line indicates the contributions of single peaks to the total spectrum.

The measured differential cross sections for the elastic and inelastic scattering to the first 2^+ and 4^+ states and to the second 2^+-state are shown in fig. 3. The data were taken in 0.5° steps up to about 50°(lab) where the oscillation pattern is clearly damped. The quoted error bars include the uncertainty due to finite angular acceptance which has been transformed into a cross section error. Especially in the region of the deep minima this "angular uncertainty" is dominating when compared to the statistical error which is smaller than 1 % for the elastic cross section at $\theta < 30^{o}$ even at the minima. From purely experimental considerations (foil thickness, detector solid angle, beam current) the absolute scale of the cross section is determined to within ca. 10 %. Finally we have normalized our data at most forward angles to the optical model results of elastic scattering as optical model calculations show very little variation in magnitude at small angles for any reasonable description of the elastic scattering cross section.

3. Elastic Scattering Analysis

The conventional optical model analysis of the elastic scattering using the standard Saxon-Woods-form (with volume absorption) for the nuclear potential

$$U(r_\alpha) = - V_o(1 + e^{x_v})^{-1} - i\ W_o(1 + e^{x_w})^{-1}$$
$$x_{v,w} = (r_\alpha - r_{v,w} \cdot A^{1/3})/a_{v,w} \qquad (3.1)$$

and a Coulomb potential from a uniformly charged sphere with $R_c = 1.3 \cdot A^{1/3}$ results in

$$J_R = \frac{V_o \pi}{A} \int_o^\infty f(r_\alpha)\ r_\alpha^2\ dr = \left| \frac{4}{3} V_o \pi R_v^3 \left[1 + (\frac{\pi a_v}{R_v})^2\right] /4A \right| = 318.6 \text{ MeV fm}^3$$

based on the parameter set given in tab. 1.

As known from previous studies such a parameter set seems to be favored for higher α-particle energies. In the present analysis we did not look very systematically for alternative parameter families. In general, studies of the ambiguities require data of a larger angular range exceeding the diffraction region. This was out of the scope of our present investigation.

A more microscopic description of the elastic α-particle-nucleus scattering starts with the intuitive expression

$$U_R(\vec{r}_\alpha) = \int \rho_m\,(\vec{r})\; V_{eff}(\vec{r}_\alpha-\vec{r})\; d^3r \qquad (3.2)$$

for the real central interaction potential, where $\rho_m(\vec{r})$ is the nucleon (centers) density distribution and $V_{eff}(\vec{r}_\alpha-\vec{r})$ an adequate effective α-particle-bound nucleon interaction. We use the Gaussian interaction proposed by Bernstein (1969) (cf Bernstein and Seidler 1971, 1972)

$$V_{eff} = \lambda_R\, V_o\, \exp(-\,|\vec{r}_\alpha - \vec{r}|^2/\mu^2) \qquad (3.3)$$

with V_o = 37 MeV and μ = 2.0 fm. The parameter λ_R takes into account the "renormalization" due to the presence of the other bound nucleons. Its value is determined phenomenologically thus absorbing some uncertainties. Preceding investigations (Bernstein and Seidler 1971, Lerner et al. 1972) on α-particle scattering from ^{40}Ca yielded $\lambda_R = 0.92 \pm 0.1$ for α-particles of E_{lab}=104 MeV. We repeated such studies of λ_R on the basis of our own data for seven (N=Z)- nuclei (Gils and Rebel 1974b) resulting in a value $\lambda_R = 0.86 \pm 0.06$. However, as discussed by Gils and Rebel (1974b) it seems reasonable to us finally to fit λ_R simultanously with size and shape parameters for every individual nucleus.
For our analysis the nucleon density distribution is assumed to have a Fermi form

$$\rho_m = \rho_o\,\left[1 + \exp((r-c_m)/a_m)\right]^{-1} \qquad (3.4)$$

and to be identical for neutrons and protons ($\rho_m \equiv \rho_p \equiv \rho_n$). The folded potential U_R (eq. 3.2) replaces the real part of the standard optical potential (eq. 3.1); in most cases the imaginary potential representation of eq. 3.1 remains unchanged (procedure A). In order to get a feeling of the influence of this representation we used alternatively Bernstein's representation (procedure B)

$$U_I(r_\alpha) = (\lambda_I/\lambda_R)\ U_R(r_\alpha) \qquad (3.5)$$

The results are compiled in tab. 1 and displayed in fig. 4. In the first run, the matter parameters c_m and a_m were fixed to corresponding values of the charge distribution. Elton and Swift (1964) investigated the charge density distribution of ^{56}Fe by electron scattering. Assumming a two-parameter Fermi shape (eq.3.4) they obtained

$$\langle r^2\rangle_{ch}^{1/2} = 3.75\ \mathrm{fm} \quad c_{ch} = 4.00\ \mathrm{fm} \quad a_{ch} = 0.57\ \mathrm{fm}$$

These values c_{ch} and a_{ch} can be related to the corresponding parameters of a Fermi shaped nucleon (= proton) density distribution in the following way: The rms-radius $\langle r^2\rangle_{ch}^{1/2}$ of the charge distribution is converted to the rms-radius of the proton (centers) distribution $\langle r^2\rangle_p^{1/2}$ via the relation

$$\langle r^2\rangle_{ch} = \langle r^2\rangle_p + \langle r^2\rangle_{s.p.} \qquad (3.6)$$

where $\langle r^2\rangle_{s.p.}^{1/2} = 0.8$ fm is the rms-radius of the charge distribution of a single proton. The difference in rms-radiis of the charge distribution and of the distribution of the protons'centers now can be ascribed to a change in the diffuseness value $a_{ch} \to a_m$ setting $c_m = c_{ch}$, or to a change of $c_{ch} \to c_m$ fixing $a_{ch} = a_m$, alternatively. Using $a_m = a_{ch} = 0.57$ fm the values extracted from electron scattering correspond to

$$c_m = 3.85\ \mathrm{fm} \quad \text{and} \quad \langle r^2\rangle_m^{1/2} = 3.66\ \mathrm{fm}$$

With that fixed values the parameters W_o, r_w and a_w were varied to find a minimum in χ^2 per degree of freedom.

In the second step we did not restrict us to matter values given but we allowed both c_m and a_m (and finally λ_R, too) to vary thus determining these parameters independent from other measurements. Detailed studies showed (Gils et al. 1974a, 1974b) that the differential cross sections are not sensitive to the particular choice of c_m and a_m, provided that the combination reproduces the correct value of the rms-radius.

The folding model analysis of elastic scattering results in

$$c_m = 3.84 \pm 0.06 \text{ fm} \qquad a_m = 0.57 \pm 0.01 \text{ fm}$$

$$\langle r^2 \rangle_m^{1/2} = 3.64 \pm 0.06 \text{ fm}$$

The value of the rms-radius $\langle r^2 \rangle_m^{1/2}$ of the nucleon distribution corresponds to $\langle r^2 \rangle_{n\,m}^{1/2} = 3.73 \pm 0.06$ fm for the nuclear matter distribution which is the quantity comparable to the charge distribution.

4. Inelastic Scattering

The macroscopic approach to the description of inelastic scattering is based on the assumption that the interaction potential follows the deformation of the nuclear surface. In the traditional "extended optical model" the interaction potential is represented by a deformed complex potential the size and shape of which is parametrized by introducing an expansion in spherical harmonics for the radius parameter ($r_{v,w}$ in expression (3.1)). Since we are mainly interested in the deformation of the nuclear surface rather than of the optical potential, we applied the folding concept to the inelastic scattering analysis, too. For this purpose we introduced into the relation (3.2) a deformed nucleon density distribution with an angular dependent nuclear radius. The nucleon density distribution was assumed to have Fermi shape and the Gaussian form of the effective interaction (eq. 3.3) with the parameter values λ_R, V_o and μ given in sect. 3 was used. For the imaginary part of the optical potential we chose the macroscopic Saxon-Woods form enabling the geometry and depth to be independent of the real potential. The deformation of the imaginary potential was fixed to the values resulting from the calculation using the extended optical potential described above.

The calculation of the differential cross sections for the various states was performed by a coupled channel method. It takes explicitely into account the higher order excitation processes due to the strong coupling among the states. Coulomb excitation is considered by a potential which is deformed corresponding to the nuclear one. The numerical calculations were carried out with a modified version (Schweimer and Raynal 1973) of the code ECIS which includes the fitting procedure.

4.1. Symmetric Rotational Model

The axially symmetric rotator model was applied to the scattering from the 0^+ (ground state), 2_1^+ and 4_1^+ states at 0., 0.847 and 2.09 MeV excitation energy. The half-way radius R of the complex potential (Saxon-Woods form) or of the nucleon density distribution is parametrized in the body fixed system by

$$R(\vartheta') = R_o(1 + \beta_2 Y_{20}(\vartheta') + \beta_4 Y_{40}(\vartheta')) \qquad (4.1)$$

The differential cross sections were simultaneously fitted in a $0^+-2_1^+-4^+$ coupling scheme, starting from the results obtained in the elastic scattering analysis. The result is shown in fig. 5, the final parameter values are quoted in table 2. The results indicate prolate deformation of the ^{56}Fe nucleus with a very small hexadecapole contribution. As exspected the folding model requires smaller values for the size and shape parameters c, a and β_2. A more detailed study on prolate-oblate effects and on the dependence of the deformation parameters β_2, β_4 from adopted size parameters c, a is given in ref. (Gils et al.1974a). From tab. 2 we extract the rms-radius $\langle r^2\rangle_m^{1/2}$ and the intrinsic quadrupole (Q_{20}) and hexadecapole (Q_{40}) moments calculated for the real potential and the nucleon density distribution.

$\langle r^2\rangle_{Pot}^{1/2} = 4.81 \pm 0.05$ fm $\quad Q_{20}^{Pot} = +116 \pm 5$ e fm^2 $\quad Q_{40}^{Pot} = +570 \pm 50$ e fm^4

$\langle r^2\rangle_{m}^{1/2} = 3.70 \pm 0.04$ fm $\quad Q_{20}^{m} = +\ 95 \pm 4$ e fm^2 $\quad Q_{40}^{m} = +450 \pm 40$ e fm^4

In order to compare these results with charge rms-radii and multipole moments we again convert the values to values of a nucleon matter distribution according to eq. (3.6). Now the difference in rms-radii can be ascribed to a change of c_m, a_m or of the deformation parameters β_l. For simplicity and consistency we assume the deformation and diffuseness to be unchanged and change only the half-way radius. Thus we obtain

$\langle r^2\rangle_{nm}^{1/2} = 3.78 \pm 0.04$ fm $\quad Q_{20}^{nm} = +100 \pm 4$ e fm^2 $\quad Q_{40}^{nm} = +500 \pm 40$ e fm^4

4.2. Asymmetric Rotational Model

Suggested by results of the generalized collective model (Rebel et al. 1974), we analyzed the scattering from the 0^+, 2_1^+, 4_1^+ and 2_2^+ states in the framework of a triaxial deformed rotator with pure quadrupole deformation (Davydov and Filippov 1958). The radius parameter R of the interaction potential or of the nucleon density distribution, respectively, is characterized in the intrinsic frame by

$$R(\vartheta',\varphi') = R_o \{1 + \sum_{\mu=0,\pm 2} a_{2\mu} Y_{2\mu}(\vartheta',\varphi')\} \qquad (4.2)$$

Usually one describes the deviation from axial symmetry by the asymmetry angle γ and a deformation parameter ß which corresponds to the quadrupole deformation $ß_2$ in the limit of vanishing asymmetry. The relations between these parameters are

$$a_{20} = ß \cos\gamma ;\ a_{22} = a_{2-2} = \frac{1}{\sqrt{2}} ß \sin\gamma = a_{20} \frac{1}{\sqrt{2}} \tan\gamma \qquad (4.3)$$

In this model the collective wave functions for the n-th state

$$|IM;n\rangle = \sum_{K=even} A_K^{(n)} \Phi_{MK}^{I}(\vec{s})$$

are superpositions of states of different K quantum numbers. The mixing amplitudes $A_K^{(n)}$ are functions of the asymmetry angle γ. Thus the deviation from axial symmetry enters the scattering both via the ratio a_{22}/a_{20} and via the amplitudes $A_K^{(n)}$. As e.g. shown in ref. (Rebel et al. 1973a) the asymmetry angle γ and the energy scale factor (containing a mass parameter and the deformation parameter ß) can be determined by fitting the level spectrum. A fit to the states 2_1^+, 2_2^+, 3^+, and 4_1^+ with equal weight on each state resulted in $\gamma = 19{,}6^o$. The experimental and calculated excitation energies and the mixing amplitudes for various different γ-values are given in tab. 3.

Recently, Abecasis and Hernândez (1972) worked out an asymmetric rotator model with a variable moment of inertia. We varied the asymmetry angle γ and the softness parameter ρ of this model to fit the energy level positions. The fit resulted in nearly the same asymmetry angle ($\gamma = 19.0^{o}$) as in the rigid Davydov-Filippov model. The parameter ρ has been found to be $\rho = 6 \cdot 10^{-3}$ indicating the softness of ^{56}Fe. This corroberates the information extracted from the collective energy surface reported in ref (Rebel et al. 1974).

Fig. 6 shows the measured and calculated angular distributions of the 0^{+}, 2_{1}^{+}, 4_{1}^{+} and 2_{2}^{+} states based on a coupled channel calculation including the folding procedure with parameter values given in line 2 of tab. 4. In some additional calculations, we tried to use various different γ-values between 10^{o} and 28^{o}. In the lower left hand part of fig. 6 the χ^{2}-values of these runs are plotted. The minimum is at $\gamma = 19^{o}$. Potential parameters and the deformation ß were fixed during the scan. A 6-parameter fit at $\gamma = 10^{o}$ (tab. 4, line 3) shows that the χ^{2}-value does not change significantly when varying the potential parameters. Looking on the partial χ^{2}-values (tab. 5) concerning the different states, it is obvious that the minimum mainly arises from a better description of the 2_{2}^{+}-state. The calculated angular distribution of the 2_{2}^{+} state for $\gamma = 10^{o}$ (dashed line in fig. 6) indicates the sensitivity to the γ-value. From the parameter values given in tab. 4 we quote the following results

$\beta = 0.241$ $\gamma = 19^{\circ}$

$\langle r^2 \rangle_m^{1/2} = 3.77 \pm 0.06$ fm $Q_{20}^{m} = 101 \pm 2$ e fm^2 $Q_{22}^{m} = 20.2 \pm 0.4$ e fm^2

$\langle r^2 \rangle_{nm}^{1/2} = 3.85 \pm 0.06$ fm $Q_{20}^{nm} = 106 \pm 2$ e fm^2 $Q_{22}^{nm} = 21.2 \pm 0.4$ e fm^2

5. Summary

Completing recent studies of the collective behavior of even f-p-shell nuclei (Rebel et al. 1972, 1973b) we have experimentally investigated the scattering of 104 MeV α-particles from ^{56}Fe. The measured differential cross sections have been analyzed in terms of coupled channels on the basis of a symmetric and a triaxial rotator model. We mainly were interested in the deformation of the nuclear matter density distribution and tried to extract from the data intrinsic multipole moments and values of the transition probabilities for ^{56}Fe. The traditional way describing inelastic scattering on the basis of a macroscopic, phenomenologically deformed optical potential provides information on the deformation of the interaction potential which is affected by the finite size of the projectile. Indeed, the values of the deformation parameters obtained in the framework of the usual extended optical model are different e.g. for α-particle and proton scattering. The deformation parameters of the interaction potential reflect only roughly the deformation of the density distribution of the target nucleus. Therefore, we used for our analysis a semi-microscopic folding model which relates the differential cross sections in a more direct way to size and shape of target nucleus. The folding model generates the interaction potential by averaging an effective α-bound nucleon interaction over a deformed distribution of the target nucleons. Such an interaction is used in the coupled channel analysis fitting the measured cross sections

by adjusting the size and shape parameters of the nucleon distribution. This procedure has been successfully applied in several preceding investigations. The following details of the procedure used in the present paper should be remarked:

(i) Contrary to other authors (Lerner et al. 1972, Bernstein and Seidler 1971, 1972) we find it reasonable to determine the phenomenological parameter λ_R for every invidual target nucleus separately,as λ_R may also reflect some structure effects.

(ii) Exchange effects which sometimes are discussed (Bimbot et al. 1973) have not been explicitely included in the present analysis. Preliminary calculations showed that they are of minor importance for the diffraction region of the angular distribution and may be already absorbed by the phenomenological adjustment of the effective α-nucleon interaction.

(iii) Converting our results of the nucleon distribution to the nuclear matter distribution which is comparable to the charge distribution we use for the rms-radius of a single neutron $\langle r^2\rangle^m_{s.n.}$ the proton value $\langle r^2\rangle^m_{s.p.} = 0.64$ and ascribe the difference between nucleon and nuclear matter distribution to the half way radius of the underlying functional form of the distribution. In this way rms-radii and intrinsic multipole moments are calculated by numerical integration over the deformed distribution.

We quote as final results:

A) Analysis of the ground-state band: Symmetric Rotator Model

$Q_{20} = + 100 \pm 4$ e fm^2 $\qquad$ $Q_{40} = 500 \pm 40$ e fm^4

$Q_{2_1^+} = -28.5 \pm 1.1$ e fm^2

$B(E2;\ 0^+ \rightarrow 2^+) = 990 \pm 80\ e^2\ fm^4$

$B(E4;\ 0^+ \rightarrow 4^+) = (4.4 \pm 0.4) \cdot 10^4\ e^2\ fm^8$

B) Analysis including the second 2^+-state: Asymmetric Rotator Model *)

$\beta = 0.241 \quad \beta_{eff} = 0.216 \quad \gamma = 19^o$

$Q_{20} = +106 \pm 2$ e fm^2 $\qquad$ $Q_{22} = 21.2$ e fm^2

$Q_0 = + 101 \pm 2$ e fm^2

$Q_{2_1^+} = -28.9 \pm 0.6$ e fm^2 $\qquad$ $Q_{2_2^+} = - Q_{2_1^+}$

$B(E2;\ 0^+ \rightarrow 2^+) = 1010 \pm 40\ e^2\ fm^4$

It is conspicuous that the asymmetric rotator model analysis which reveals a triaxial deformation of $\gamma \approx 20^o$ has little effect to the values of quadrupole moment $Q_{2_1^+}$ extracted by the symmetric rotator model analysis of the ground band.

In tab. 6 the results are compared with other experimental results.

The values extracted from helion and α-particle scattering in the framework of a deformed optical potential underestimate moments and transition probabilities compared to proton scattering and electromagnetic findings, even when - by the recipe of Bernstein (1969) - the deformation parameters are "renormalized".

---

*) β_{eff}, Q_o, and $Q_{2_1^+}$ are defined according to Davydov and Filippov (1958)

The value of the asymmetry angle γ which we obtain from our analysis is in good agreement with the results of analyses of the level spectrum of ^{56}Fe. (Davydov and Chaban 1960, Davydov and Filippov 1958, Abecasis and Hernândez 1972). A recent investigation of the collective energy surface of ^{56}Fe results in effective γ-values for the various states ranging from about 19° to 21°.

However, it should be remarked that there are significant deviations of the experimental 2_2^+-differential cross section from a pure collective description. This has been also found in a recent investigation on the basis of a more generalized collective model (Rebel et al. 1974). We ascribe the deviation to an unknown admixture to the 2_2^+-amplitude which is neglected by the collective model. Though spurious such an amplitude influences the cross section very sensitively.

Acknowledgements

We thank Dr. G. Schatz for his encouraging interest in our studies. We take the opportunity to thank Ing. F. Schulz and the cyclotron staff for their continuous effort in preparing the α-beam with excellent quality, and Miss C. Rämer and Dipl. Ing. W. Karbstein for help in using the scattering and computer facilities of the Karlsruhe Cyclotron Laboratory. We thank Miss W. Nowatzke and Mrs. V. Walsch for their assistence in data handling and preparation of the figures.

References

Abecasis S.M. and Hernândez E.S., 1972; Nucl. Phys. A180, 485

Andreyev D.S., Grinberg A.P., Erokhina K.I. and Lemberg I. Kh., 1960; Nucl. Phys. 19, 400

Bernstein A.M., 1969; Advances in Nuclear Physics, Vol. 3, ed. M. Baranger and E. Vogt, Plenum Press, New York-London p.325

Bernstein A.M. and Seidler W.A., 1971; Phys. Lett. 34B, 569

Bernstein A.M. and Seidler W.A., 1972; Phys. Lett. 39B, 583

Bimbot L., Tatischeff B., Brissaud I., Le Bornec Y., Frascaria N. and Willis A., 1973; Nucl. Phys. A210, 397

Chandra H. and Rustgi M.L., 1972; Phys. Rev. C6 1281

Davydov A.S. and Chaban A.A., 1960; Nucl. Phys. 20, 499

Davydov A.S. and Filippov G.F., 1958; Nucl. Phys. 8, 237

Elton L.R.B. and Swift A., 1964; Proc. Phys. Soc. 84, 125

Gils H.J., Rebel H. and Ciocănel A., 1974a; Rev. Roum. de Phys., in press

Gils H.J. and Rebel H., 1974b; in preparation

Gneuß G., Mosel, U. and Greiner W., 1969; Phys. Lett. 30B, 397

Gneuß G., Mosel, U. and Greiner W., 1970; Phys. Lett. 31B, 269

Gneuß G. and Greiner W., 1971; Nucl. Phys. A71, 449

Kelly W.H. and Beard G.B., 1961; Nucl. Phys. 27, 188

Lerner G.M., Hiebert J.C., Rutledge L.L. and Bernstein A.M., 1972; Phys. Rev. C6, 1254

Lesser P.M.S., Cline D., Goode P. and Horoshko R.N., 1972; Nucl. Phys. A190, 597

Mani G.S., 1971; Nucl. Phys. A165, 225

Marchese C.J., Clarke N.M. and Griffiths R.J., 1973; Nucl. Phys. A202, 421

Metzger F.R., 1961; Nucl. Phys. 27, 612

Parikh J.K., 1972; Phys. Lett. 41B, 271

Peterson R.J., 1969; Ann. of. Phys. 53, 40

Rebel H., 1972; Nucl. Phys. A180, 332

Rebel H., Löhken R., Schweimer G.W., Schatz G. and Hauser G., 1972a; Z. Phys. 256, 258

Rebel H., Schweimer G.W., Schatz G., Specht J., Löhken R., Hauser G., Habs D. and Klewe-Nebenius H., 1972b; Nucl. Phys. A182, 145

Rebel H. and Habs D., 1973a; Phys. Rev. C8, 1391

Rebel H., Hauser G., Schweimer G.W., Nowicki G., Wiesner W. and Hartmann D., 1973b; Nucl. Phys. A218, 13

Rebel H., 1974; Kernforschungszentrum Karlsruhe, report KFK 2065

Rebel H., Schweimer G.W., Habs D. and Gils H.J., 1974; Nucl. Phys. A225, 457

Schweimer G.W., Raynal J., 1973; preprint and private communications

Stelson P.H. and Grodzins L., 1965; Nucl. Data A1, 21

Towsley C.W., Cline D. and Horoshko R.N., 1972; Nucl. Phys. A204, 574

V_o [MeV]	r_v [fm]	a_v [fm]	W_o [MeV]	r_w [fm]	a_w [fm]	$\langle r^2\rangle^{1/2}_{Pot}$ [fm]	χ^2/F		
114(1)	1.31(1)	0.71(1)	21.4(4)	1.58(1)	0.61(2)	4.69(6)	5.5	macroscopic optical potential 6 parameters varied	
λ_R	$c_m A^{-1/3}$ [fm]	a_m [fm]	W_o [MeV]	r_w [fm]	a_w [fm]	$\langle r^2\rangle^{1/2}_m$ [fm]	χ^2/F	real parameters varied	comments
0.86	1.01	0.57	26(1)	1.54(1)	0.60(2)	3.66	16.0	-	proc. A
0.86	1.037(5)	0.54(1)	26(1)	1.56(2)	0.57(1)	3.67(3)	15.6	c_m, a_m	A
0.92	1.02(2)	0.55(2)	24(1)	1.60(1)	0.54(2)	3.65(6)	10.3	c_m, a_m	A
0.900(4)	1.00(1)	0.57(2)	22.1(8)	1.60(1)	0.55(2)	3.64(6)	9.0	λ_R, c_m, a_m	A
			λ_I						
0.86	1.09(1)	0.47(2)	0.494(5)	-	-	3.67(4)	16.3	c_m, a_m	B
0.90	1.06(1)	0.48(2)	0.514(6)	-	-	3.61(4)	16.4	c_m, a_m	B

Tab. 1: Results of the elastic scattering analysis. Procedure A of the folding model uses a macroscopic imaginary potential the three parameters of which are all varied. The numbers in brackets are the standard errors in the last digit of the quoted values. The procedure of determination of the errors is given in ref. (Rebel et al. 1972b).

V_o [MeV]	r_v [fm]	a_v [fm]	W_o [MeV]	r_w [fm]	a_w [fm]	β_2	β_4	$\langle r^2\rangle^{1/2}_{Pot}$ [fm]	χ^2/F	
108.(2)	1.348(8)	0.71(1)	21.7(7)	1.61(1)	0.50(1)	0.178(2)	0.009(4)	4.81(5)	14.4	extended optical potential

λ_R	$c_m A^{-1/3}$ [fm]	a_m [fm]	W_o [MeV]	r_w [fm]	a_w [fm]	β_2	β_4	$\langle r^2\rangle^{1/2}_m$ [fm]	χ^2/F	real parameters varied	comments
0.86	1.01	0.57	18.3(6)	1.60(1)	0.58(2)	0.256(3)	0.02(1)	3.71	24.0		proc.A
0.86	1.23(2)	0.32(4)	28(3)	1.59(1)	0.47(2)	0.208(5)	0.011(6)	3.88(4)	18.4	c_m, a_m	A
0.92	1.06(2)	0.51(2)	18.5(9)	1.63(1)	0.52(1)	0.239(4)	0.019(8)	3.71(4)	15.5	c_m, a_m	A
0.950(8)	1.04(2)	0.53(2)	18(1)	1.65(1)	0.49(1)	0.238(5)	0.026(9)	3.70(4)	14.3	λ_R, c_m, a_m	A
			λ_I								
0.95	1.09(1)	0.43(2)	0.454(4)	-	-	0.237(4)	0.036(7)	3.65(4)	19.0	c_m, a_m	B

Tab. 2: Results of the symmetric rotator coupled channel analysis ($0^+ - 2^+_1 - 4^+$ - coupling). In all cases the deformation parameters and the imaginary potential parameters were varied. The numbers in brackets indicate the standard errors in the last digit.

I	E_n^{exp} [MeV]	E_n^{th} [MeV]	$A_o^{(n)}$	$A_2^{(n)}$	$A_4^{(n)}$	
2_1^+	0.847	0.690	0.9968	0.0797		$\gamma = 19.6^o$ obtained by fitting the energy levels
2_2^+	2.66	2.70	-0.0797	0.9968		
3^+	3.45	3.39	0.0	1.0		
4_1^+	2.09	2.17	0.9612	0.2758	0.0083	
2_1^+		0.641	0.9993	0.0377		$\gamma = 16^o$ fixed
2_2^+		3.84	-0.0377	0.9993		
3^+		4.48	0.0	1.0		
4_1^+		2.09	0.9899	0.1418	0.0020	
2_1^+		0.762	0.9821	0.1885		$\gamma = 24^o$ fixed
2_2^+		1.97	-0.1885	0.9821		
3^+		2.73	0.0	1.0		
4_1^+		2.21	0.8758	0.4816	0.0331	

Tab. 3: Different sets of mixing amplitudes resulting from the asymmetric rotator description of the ^{56}Fe level spectrum

V_o [MeV]	r_w [fm]	a_w [fm]	W_o [MeV]	r_w [fm]	a_w [fm]	a_{20}	γ	$\langle r^2\rangle^{1/2}_{Pot}$ [fm]	χ^2/F		
107(2)	1.357(8)	0.70(1)	22(1)	1.61(1)	0.51(2)	0.176(2)	19.6	4.82	17.2	extended optical model 7 parameters varied	
λ_R	$c_m A^{1/3}$ [fm]	a_m [fm]	W_o [MeV]	r_w [fm]	a_w [fm]	a_{20}	γ	$\langle r^2\rangle^{1/2}_m$ [fm]	χ^2/F	real parameters varied	comments
0.93(3)	1.16(1)	0.38(2)	28(3)	1.56(2)	0.52(2)	0.227(5)	19.6	3.77(6)	20.6	λ_R, c_m, a_m	proc. A
0.96(1)	1.09(1)	0.48(3)	18(2)	1.66(2)	0.47(2)	0.227	10^o	3.73(6)	25.9	λ_R, c_m, a_m	A a_{20} fixed
			λ_I								
0.93	1.10(1)	0.43(2)	0.449(9)	-	-	0.225(4)	19.6	3.69(6)	21.2	c_m, a_m	B

Tab. 4: Triaxial rotator analysis ($0^+ - 2_1^+ - 4^+ - 2_2^+$ - coupling). In all cases the imaginary potential parameters were varied. The numbers in brackets indicate the standard errors in the last digit.

γ	χ^2/F (total)	χ^2/F (0^+)	χ^2/F (2_1^+)	χ^2/F (4_1^+)	χ^2/F (2_2^+)
10	28.2	19.3	25.5	7.3	79.9
14	23.0	19.7	24.2	7.1	47.9
17	20.5	18.2	24.7	5.5	35.5
18	20.2	18.0	24.9	5.4	33.9
19	20.1	17.8	25.2	5.2	33.4
19.6	20.2	17.7	25.4	5.2	33.6
21	20.4	17.4	25.7	4.9	35.5
24	22.3	16.8	26.2	4.3	48.3
28	28.3	16.2	27.2	3.8	88.0

Tab. 5: Total and partial χ^2-values per degree of freedom for different asymmetry angles γ. In all cases the potential parameters were fixed to the values of tab. 4, line 2 and the parameter ß was set to ß = 0.241.

Method	Reference	β_2	Q_{20} [e fm^2]	$Q_{2_1^+}$ [e fm^2]	B(E2)↑ [e^{2}fm^4]	B(E2)↑/B(E2)$_{s.p.}$
Electromagnetic (average)	Stelson and Grodzins (1965)	0.23	(95)	(27)	900 ± 100	14.1 ± 1.6
Electromagnetic (reorientation)	Lesser et al. 1972		$(+87\pm20)$	-24.9 ± 5.8	970 ± 20	15.2 ± 0.3
p,p' (average)	Peterson 1969		(102)	(29)	1030 ± 300	16.2 ± 4.7
p,p'; DWBA	Main 1971	0.20 ± 0.02	(90)	(26)	810 ± 100	12.7 ± 1.6
^{3}He;α (average)	Peterson 1969		(84)	(24)	700 ± 70	11.0 ± 1.1
^{3}He,^{3}He'; CC	Marchese et al.1973	0.21	(79)	(23)	623*)	9.8
α,α'; DWBA	Bernstein 1969		(89 ± 6)	(26 ± 2)	792 ± 121	12.4 ± 1.9
α,α'; CC, Folding, SR	present experiment	0.238	$+100\pm4$	(-28.5 ± 1.2)	(990 ± 80)	15.6 ± 1.3
α,α'; CC, Folding, ASR	present experiment	β = 0.241	$Q_o=+101\pm2$	(-28.9 ± 0.6)	(1010 ± 40)	15.9 ± 0.6

Tab. 6: Comparison of deformation parameters, quadrupole moments and transition probabilities of ^{56}Fe obtained by different experimental methods. Values in brackets are deduced from B(E2)-values given by the relations $Q_{20} = \sqrt{\frac{16\pi}{5}\, B(E2)\uparrow}$ and $Q_{2_1^+} = -\frac{2}{7}\, Q_{20}$. In the case of the asymmetric rotator analysis (ASR) the parameters β and Q_o are comparable to β_2 and Q_{20}

*) Calculated from β_2 and R_v by the method given by Bernstein (1969).

Figure Captions

Fig. 1: Set-up of the electronics. The numbers correspond to the producers' type identifications of the NIM-modules used (BA: Canberra; all the others: Ortec).

Fig. 2: Energy spectrum of the outgoing α-particles from $^{56}Fe(\alpha,\alpha')^{56}Fe$. The dashed line indicates the contribution of a single peak to the whole spectrum.
The states at -2.96, -3.125 and -3.37 MeV are only analyzed for background considerations.

Fig. 3: Experimental differential cross sections: $^{56}Fe(\alpha,\alpha')^{56}Fe$. The theoretical curve represents the result of the conventional optical model analysis of elastic scattering. This paper is not engaged in the angular distribution of the 3^- state shown.

Fig. 4: Folding model analysis of elastic scattering. In the inserted χ^2- contour plot over the c_m-a_m-plane the correlation between these two parameters is demonstrated. The full line shows the corresponding values of c_m and a_m for $\chi^2 = 1.5 \cdot \chi^2_{min}$. The dashed straight lines mark constant rms-radii and the bend dashed line follows the valley of minimal χ^2/F for given a_m shown in the second inserted graph.

Fig. 5: Symmetric rotator model analysis of inelastic scattering using the folding procedure. The parameters of the interaction potentials are given in tab. 2 (line5).

Fig. 6: Triaxial rotator model analysis of inelastic scattering using the folding procedure. The dashed 2_2^+ angular distribution corresponds to $\gamma = 10^o$. Interaction potential parameters are given in tab. 4 (line2). The inserted graph shows the curve of the χ^2-values per degree of freedom over the asymmetry angle γ.

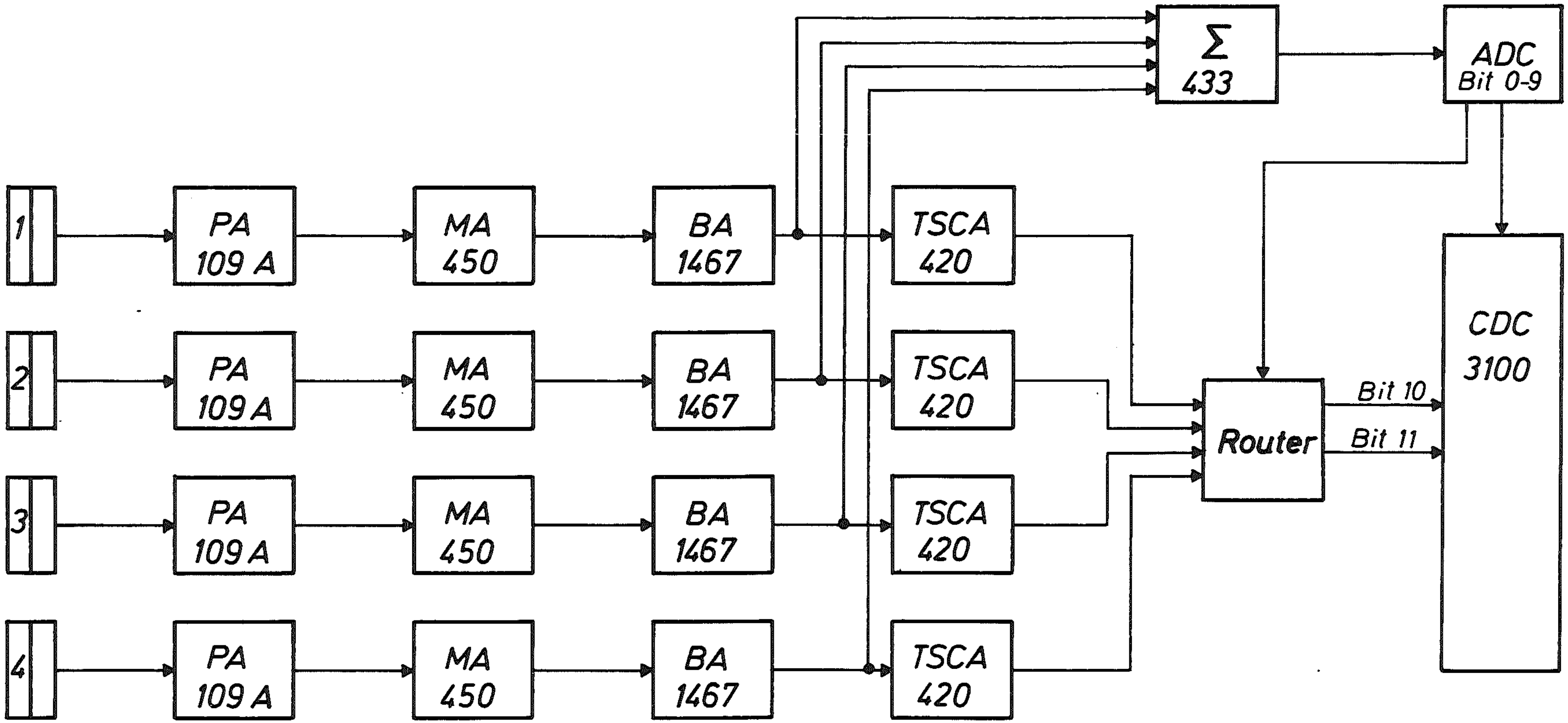

Zykl. 30.10.74

Fig. 1

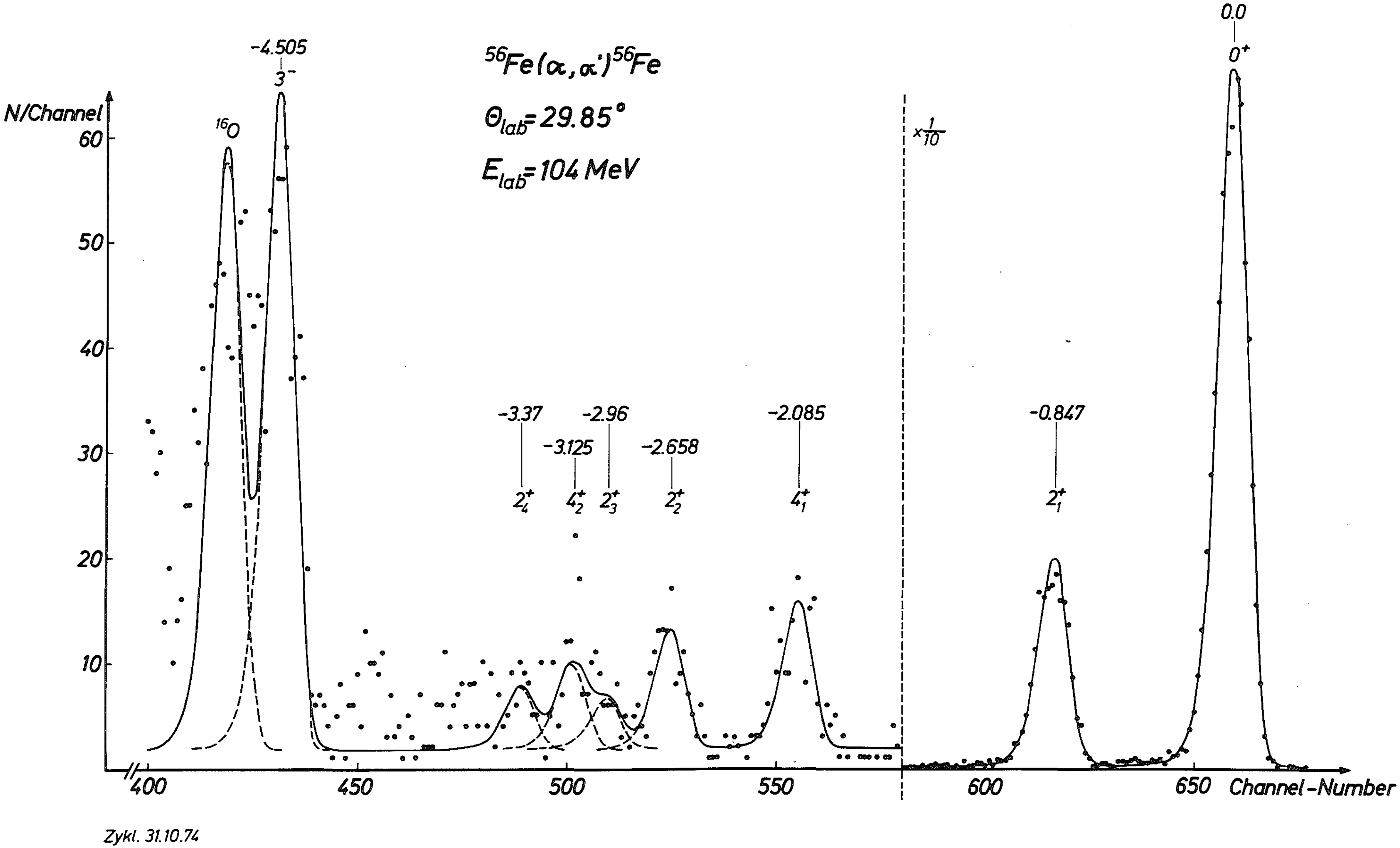
$^{56}Fe(\alpha,\alpha')^{56}Fe$
$\Theta_{lab}=29.85°$
$E_{lab}=104$ MeV
N/Channel
60
50
40
30
20
10
^{16}O
-4.505
3^-
-3.37
2_4^+
-3.125
4_2^+
-2.96
2_3^+
-2.658
2_2^+
-2.085
4_1^+
$\times\frac{1}{10}$
-0.847
2_1^+
0.0
0^+
400
450
500
550
600
650
Channel-Number
Zykl. 31.10.74

Fig. 2

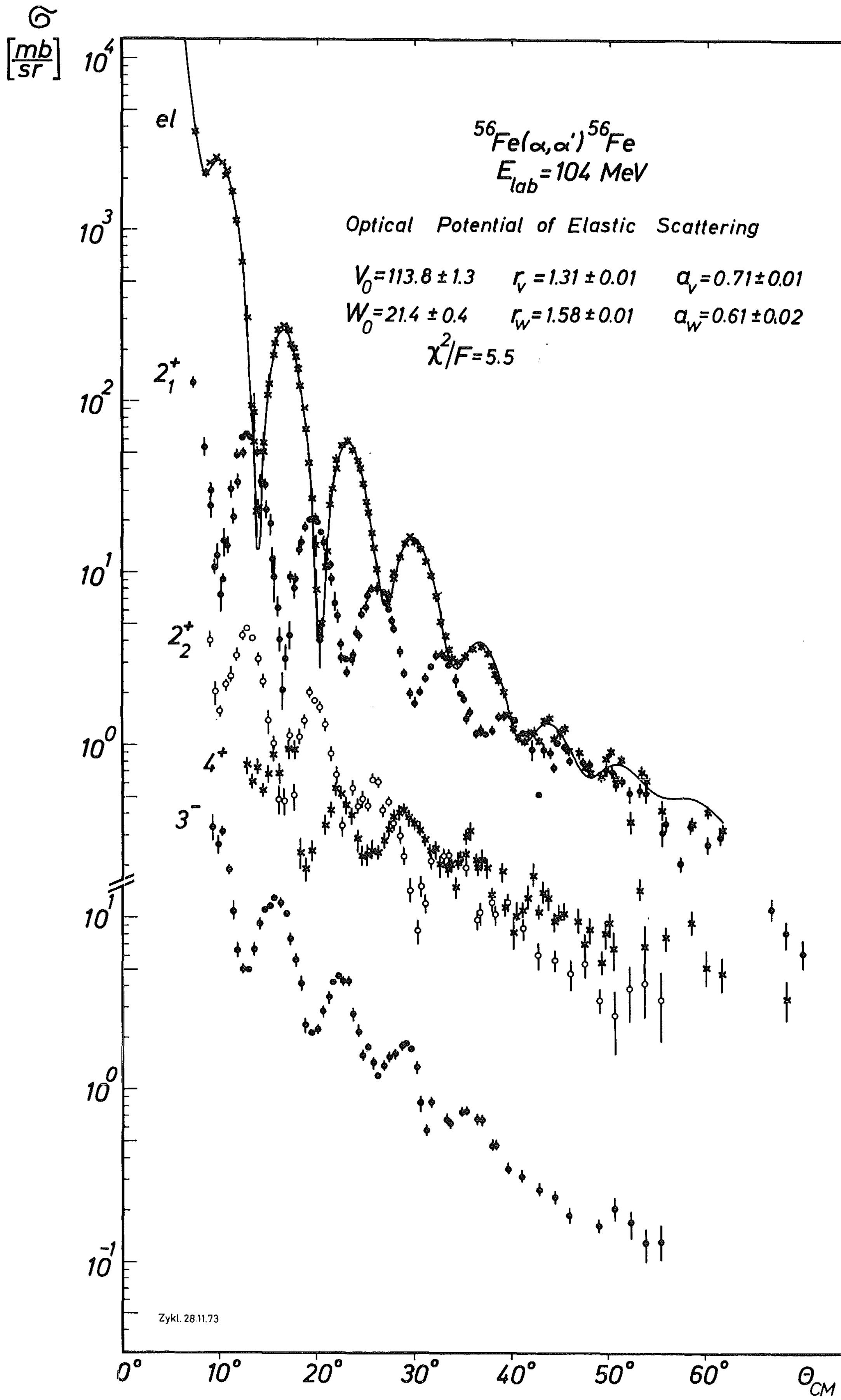

σ [mb/sr]
10^4
10^3
10^2
10^1
10^0
10^1
10^0
10^{-1}
el
2_1^+
2_2^+
4^+
3^-
$^{56}Fe(\alpha,\alpha')^{56}Fe$
$E_{lab}=104$ MeV
Optical Potential of Elastic Scattering
$V_0=113.8\pm1.3$ $r_V=1.31\pm0.01$ $a_V=0.71\pm0.01$
$W_0=21.4\pm0.4$ $r_W=1.58\pm0.01$ $a_W=0.61\pm0.02$
$\chi^2/F=5.5$
Zykl. 28.11.73
0° 10° 20° 30° 40° 50° 60°
Θ_{CM}

Fig. 3

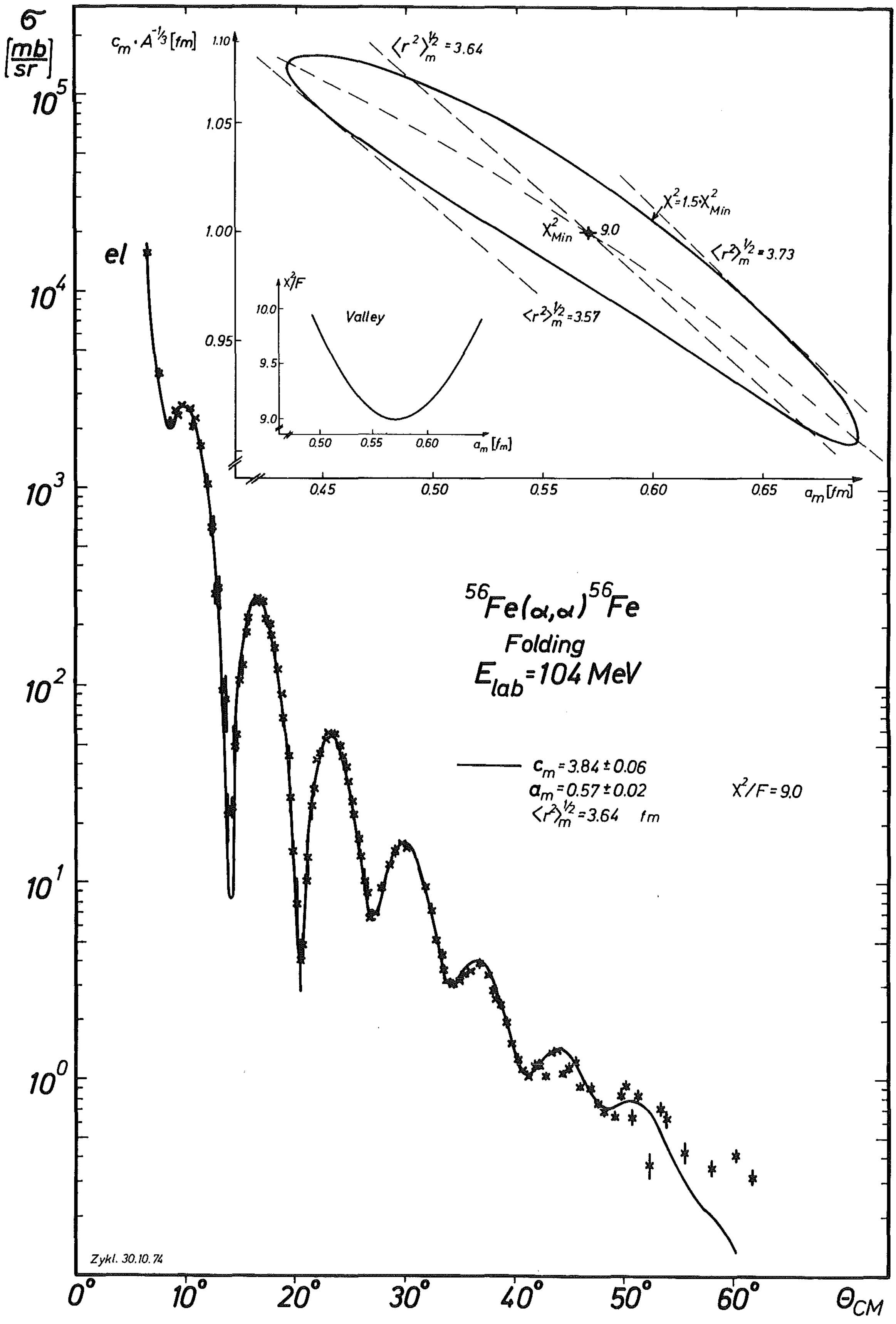

σ [mb/sr]
$^{56}Fe(\alpha,\alpha)^{56}Fe$
Folding
E_{lab}=104 MeV
c_m=3.84±0.06
a_m=0.57±0.02
$\langle r^2\rangle_m^{1/2}$=3.64 fm
χ^2/F=9.0
el
$c_m \cdot A^{-1/3}$ [fm]
$\langle r^2\rangle_m^{1/2}$=3.64
$\langle r^2\rangle_m^{1/2}$=3.73
$\langle r^2\rangle_m^{1/2}$=3.57
$\chi^2=1.5\,\chi^2_{Min}$
χ^2_{Min} 9.0
Valley
χ^2/F
a_m [fm]
Zykl. 30.10.74
Θ_{CM}

Fig. 4

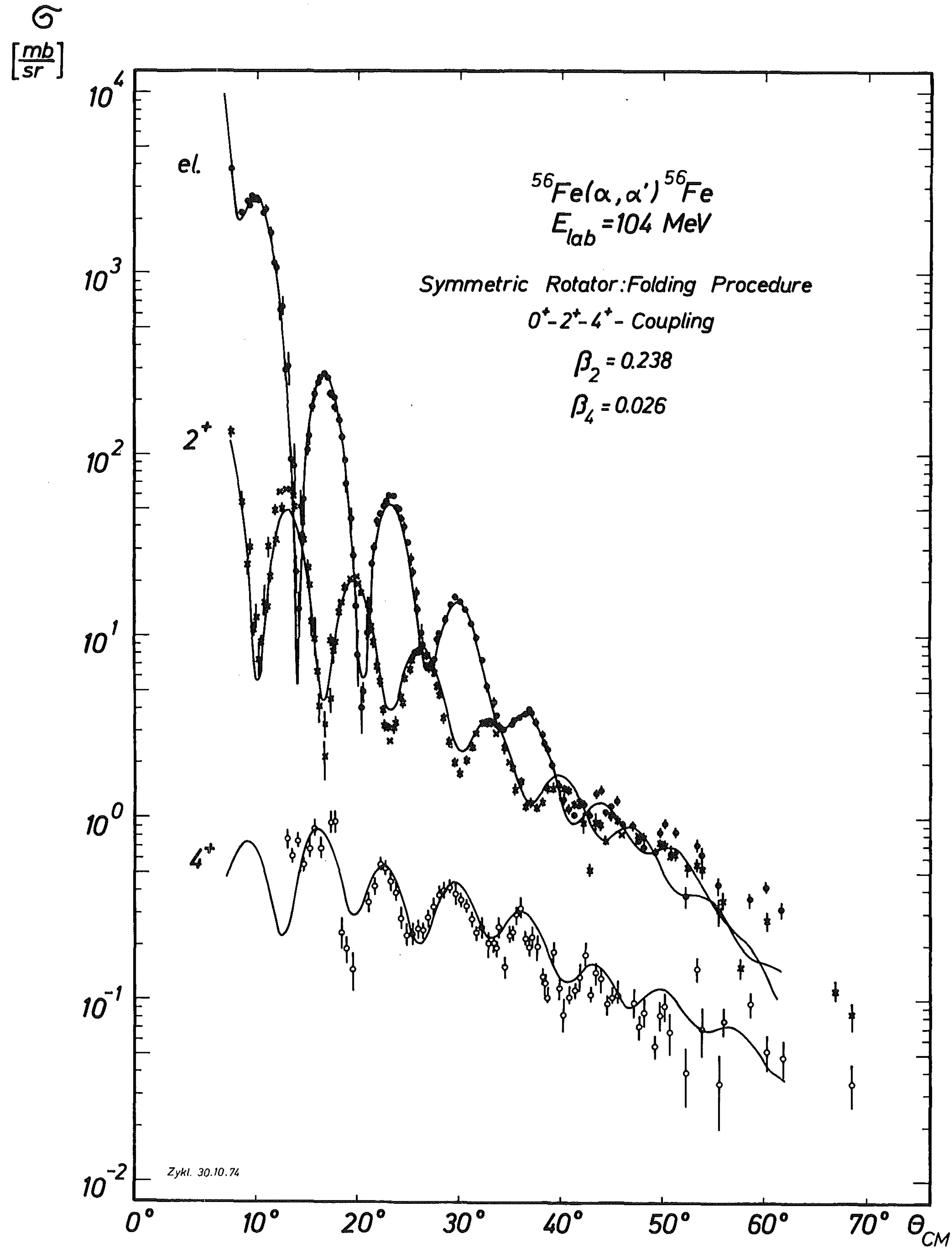
σ
[mb/sr]
10^4
10^3
10^2
10^1
10^0
10^-1
10^-2
el.
2+
4+
56Fe(α,α')56Fe
Elab=104 MeV
Symmetric Rotator:Folding Procedure
0+-2+-4+- Coupling
β2 = 0.238
β4 = 0.026
Zykl. 30.10.74
0°
10°
20°
30°
40°
50°
60°
70°
θCM

Fig. 5

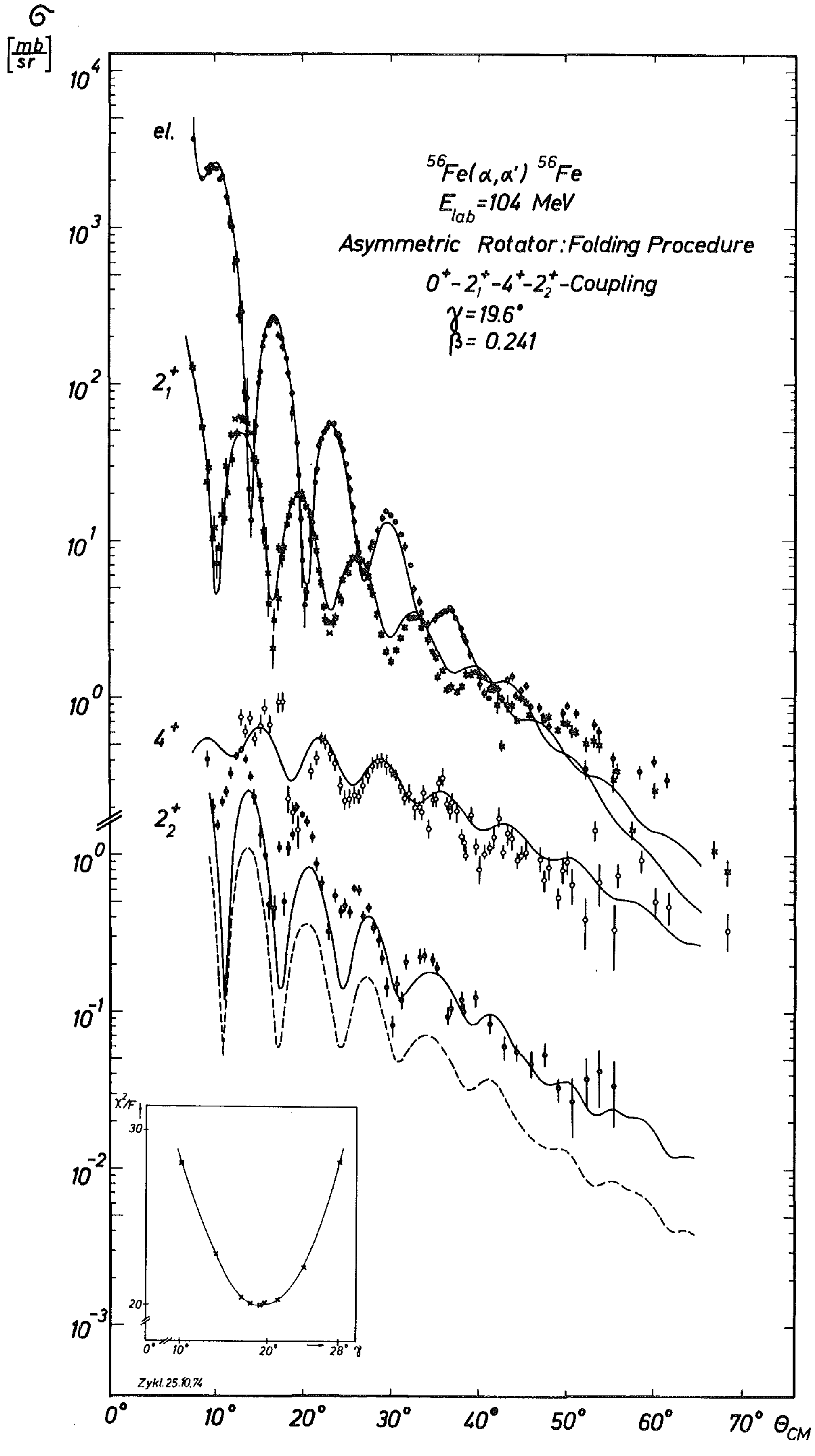

$^{56}Fe(\alpha,\alpha')\,^{56}Fe$
E_{lab}=104 MeV
Asymmetric Rotator: Folding Procedure
$0^+-2_1^+-4^+-2_2^+$-Coupling
γ=19.6°
β= 0.241
el.
2_1^+
4^+
2_2^+
σ [mb/sr]
Θ_{CM}
χ^2/F
Zykl. 25.10.74

Fig. 6

Appendix

Experimental cross sections: The quoted errors of the experimental cross sections include the error arising from the finite angular acceptance which is converted into a cross section error.

~~This paper is not engaged in the cross sections of the 3^- state given.~~

SCATTERING OF 104 MEV ALPHAPARTICLES ON 56 FE

Q = 0.0 MEV I = 0+

ECM = 97.064 MEV K = 4.1647/FERMI ETA = 1.60628

LABORATORY DATA THETA DEGREE	SIGMA MB/SR	DSIGMA %	RUTHERFORD SIGMA/SR	CM DATA THETA DEGREE	SIGMA MB/SR	DSIGMA MB/SR
6.00	1.812E 04	7.6	4.211E-01	6.44	1.574E 04	1.191E 03
7.00	4.410E 03	4.3	1.897E-01	7.51	3.832E 03	1.664E 02
8.00	2.501E 03	3.1	1.834E-01	8.58	2.174E 03	6.784E 01
8.50	2.877E 03	1.5	2.688E-01	9.12	2.501E 03	3.661E 01
8.65	2.741E 03	1.7	2.746E-01	9.28	2.383E 03	3.977E 01
9.00	3.071E 03	1.2	3.605E-01	9.66	2.670E 03	3.195E 01
9.15	2.968E 03	0.5	3.722E-01	9.82	2.581E 03	1.325E 01
9.50	2.895E 03	3.1	4.217E-01	10.19	2.518E 03	7.833E 01
9.65	2.886E 03	1.2	4.475E-01	10.35	2.510E 03	3.016E 01
10.00	2.445E 03	4.2	4.370E-01	10.73	2.127E 03	8.899E 01
10.15	2.625E 03	3.7	4.979E-01	10.89	2.284E 03	8.528E 01
10.50	1.934E 03	0.7	4.200E-01	11.27	1.683E 03	1.106E 01
10.65	1.907E 03	7.2	4.382E-01	11.43	1.659E 03	1.196E 02
11.00	1.316E 03	8.9	3.440E-01	11.80	1.145E 03	1.015E 02
11.15	1.251E 03	9.2	3.452E-01	11.96	1.089E 03	1.000E 02
11.50	7.329E 02	10.8	2.287E-01	12.34	6.380E 02	6.899E 01
11.65	7.578E 02	11.9	2.491E-01	12.50	6.597E 02	7.820E 01
12.00	3.367E 02	13.5	1.245E-01	12.87	2.932E 02	3.967E 01
12.15	3.532E 02	18.6	1.372E-01	13.03	3.076E 02	5.734E 01
12.50	1.090E 02	15.3	4.743E-02	13.41	9.494E 01	1.449E 01
12.65	9.952E 01	32.7	4.541E-02	13.57	8.669E 01	2.838E 01
13.00	2.586E 01	25.3	1.316E-02	13.94	2.253E 01	5.697E 00
13.15	2.760E 01	12.6	1.470E-02	14.11	2.405E 01	3.024E 00
13.50	5.852E 01	23.0	3.460E-02	14.48	5.100E 01	1.174E 01
13.65	6.511E 01	18.5	4.023E-02	14.64	5.675E 01	1.048E 01
14.00	1.259E 02	14.2	8.603E-02	15.02	1.097E 02	1.560E 01
14.15	1.475E 02	12.5	1.052E-01	15.18	1.286E 02	1.609E 01
14.50	2.154E 02	7.2	1.692E-01	15.55	1.878E 02	1.346E 01
14.65	2.494E 02	6.5	2.041E-01	15.71	2.175E 02	1.409E 01
15.00	2.926E 02	2.1	2.631E-01	16.09	2.552E 02	5.252E 00
15.15	3.086E 02	2.4	2.887E-01	16.25	2.692E 02	6.505E 00
15.50	3.222E 02	1.2	3.301E-01	16.62	2.811E 02	3.315E 00
15.65	3.208E 02	1.9	3.414E-01	16.78	2.799E 02	5.388E 00
16.00	3.040E 02	4.5	3.533E-01	17.16	2.653E 02	1.191E 01
16.15	2.487E 02	4.6	2.999E-01	17.32	2.171E 02	1.007E 01
16.50	2.360E 02	5.0	3.099E-01	17.69	2.061E 02	1.032E 01
16.65	2.063E 02	5.3	2.808E-01	17.85	1.801E 02	9.553E 00
17.00	1.771E 02	8.2	2.619E-01	18.23	1.547E 02	1.263E 01
17.15	1.413E 02	6.5	2.163E-01	18.39	1.234E 02	8.004E 00
17.50	1.049E 02	1.2	1.740E-01	18.76	9.166E 01	1.089E 00
17.65	7.821E 01	9.9	1.342E-01	18.92	6.835E 01	6.749E 00
18.00	5.086E 01	13.4	9.435E-02	19.30	4.446E 01	5.977E 00
18.15	3.144E 01	13.5	6.028E-02	19.46	2.749E 01	3.699E 00
18.50	1.674E 01	14.5	3.462E-02	19.83	1.464E 01	2.116E 00
18.65	9.113E 00	32.8	1.946E-02	19.99	7.970E 00	2.616E 00
19.00	4.680E 00	30.7	1.076E-02	20.37	4.094E 00	1.259E 00
19.15	5.672E 00	12.0	1.345E-02	20.53	4.962E 00	5.934E-01
19.50	1.185E 01	28.0	3.019E-02	20.90	1.037E 01	2.906E 00
19.65	1.568E 01	18.9	4.118E-02	21.06	1.372E 01	2.588E 00
20.00	2.844E 01	14.2	8.010E-02	21.44	2.490E 01	3.527E 00
20.15	3.443E 01	6.2	9.989E-02	21.60	3.015E 01	1.872E 00
20.50	4.862E 01	4.4	1.510E-01	21.97	4.259E 01	1.862E 00
20.65	5.262E 01	3.9	1.682E-01	22.13	4.610E 01	1.799E 00
21.00	5.904E 01	3.2	2.017E-01	22.51	5.174E 01	1.670E 00
21.15	6.231E 01	1.6	2.190E-01	22.67	5.461E 01	8.644E-01
21.50	6.829E 01	0.9	2.561E-01	23.04	5.987E 01	5.170E-01
21.65	6.844E 01	1.2	2.638E-01	23.20	6.001E 01	7.026E-01
22.00	6.672E 01	3.0	2.740E-01	23.57	5.852E 01	1.750E 00
22.15	5.819E 01	3.3	2.454E-01	23.73	5.104E 01	1.673E 00
22.50	5.706E 01	4.2	2.560E-01	24.11	5.007E 01	2.099E 00
22.65	5.014E 01	4.4	2.310E-01	24.27	4.400E 01	1.943E 00
23.00	4.532E 01	7.0	2.218E-01	24.64	3.979E 01	2.771E 00
23.15	3.723E 01	4.3	1.869E-01	24.80	3.269E 01	1.407E 00
23.50	2.968E 01	7.1	1.581E-01	25.17	2.607E 01	1.853E 00
23.65	2.540E 01	6.0	1.388E-01	25.33	2.231E 01	1.344E 00
24.00	1.926E 01	7.9	1.115E-01	25.71	1.693E 01	1.344E 00
24.15	1.586E 01	6.7	9.409E-02	25.87	1.394E 01	9.396E-01
24.50	1.173E 01	13.0	7.365E-02	26.24	1.031E 01	1.336E 00
24.65	1.011E 01	9.2	6.502E-02	26.40	8.890E 00	8.151E-01
25.00	7.771E 00	2.2	5.283E-02	26.78	6.836E 00	1.519E-01
25.15	7.539E 00	3.3	5.247E-02	26.94	6.633E 00	2.208E-01
25.50	7.957E 00	7.5	5.848E-02	27.31	7.003E 00	5.240E-01
25.65	8.315E 00	4.2	6.253E-02	27.47	7.320E 00	3.055E-01
26.00	1.081E 01	5.6	8.575E-02	27.84	9.520E 00	5.338E-01
26.15	1.143E 01	4.0	9.274E-02	28.00	1.007E 01	3.988E-01
26.65	1.394E 01	3.3	1.218E-01	28.53	1.228E 01	4.095E-01
27.15	1.694E 01	2.3	1.593E-01	29.07	1.494E 01	3.451E-01
27.65	1.845E 01	1.6	1.864E-01	29.60	1.628E 01	2.588E-01
28.15	1.721E 01	2.1	1.865E-01	30.13	1.519E 01	3.123E-01
28.65	1.555E 01	2.3	1.805E-01	30.66	1.374E 01	3.214E-01
29.15	1.329E 01	2.9	1.651E-01	31.20	1.175E 01	3.349E-01
29.65	1.096E 01	3.4	1.455E-01	31.73	9.693E 00	3.326E-01
30.15	8.337E 00	6.8	1.182E-01	32.26	7.378E 00	5.032E-01
30.65	5.875E 00	6.5	8.880E-02	32.79	5.202E 00	3.383E-01
31.15	4.889E 00	4.8	7.872E-02	33.32	4.332E 00	2.064E-01
31.37	4.109E 00	4.6	6.800E-02	33.56	3.642E 00	1.691E-01
31.65	3.585E 00	5.5	6.142E-02	33.85	3.178E 00	1.763E-01
32.15	3.464E 00	3.4	6.308E-02	34.39	3.073E 00	1.040E-01
32.65	3.630E 00	2.1	7.020E-02	34.92	3.223E 00	6.706E-02
32.87	3.673E 00	2.3	7.291E-02	35.15	3.262E 00	7.587E-02
33.15	3.902E 00	3.4	8.005E-02	35.45	3.466E 00	1.166E-01
33.65	4.016E 00	3.4	8.733E-02	35.98	3.570E 00	1.229E-01
34.15	4.172E 00	2.5	9.607E-02	36.51	3.711E 00	9.448E-02
34.37	4.484E 00	3.1	1.059E-01	36.74	3.990E 00	1.241E-01
34.65	4.198E 00	3.5	1.023E-01	37.04	3.737E 00	1.292E-01
35.15	3.778E 00	4.0	9.730E-02	37.57	3.366E 00	1.352E-01
35.65	3.229E 00	3.2	8.783E-02	38.10	2.879E 00	9.236E-02
35.87	2.885E 00	5.1	8.037E-02	38.33	2.573E 00	1.318E-01
36.15	2.696E 00	5.2	7.740E-02	38.63	2.405E 00	1.257E-01
36.65	2.206E 00	6.0	6.678E-02	39.16	1.970E 00	1.172E-01
37.15	1.706E 00	4.2	5.442E-02	39.69	1.524E 00	6.380E-02
37.65	1.427E 00	6.4	4.793E-02	40.22	1.276E 00	8.192E-02
38.15	1.235E 00	5.9	4.364E-02	40.74	1.105E 00	6.487E-02
38.65	1.150E 00	3.5	4.273E-02	41.27	1.030E 00	3.635E-02
39.15	1.312E 00	5.4	5.122E-02	41.80	1.176E 00	6.357E-02
39.65	1.323E 00	5.4	5.423E-02	42.33	1.187E 00	6.464E-02
40.15	1.168E 00	3.3	5.023E-02	42.86	1.048E 00	3.482E-02
40.65	1.523E 00	5.3	6.868E-02	43.39	1.368E 00	7.227E-02
41.15	1.594E 00	4.9	7.533E-02	43.91	1.433E 00	6.958E-02
41.65	1.198E 00	3.2	5.929E-02	44.44	1.078E 00	3.484E-02
42.15	1.283E 00	5.3	6.646E-02	44.97	1.156E 00	6.124E-02
42.65	1.377E 00	5.5	7.461E-02	45.50	1.241E 00	6.769E-02
43.15	1.028E 00	3.7	5.823E-02	46.02	9.274E-01	3.436E-02
44.15	1.003E 00	6.4	6.199E-02	47.08	9.064E-01	5.826E-02
44.65	8.272E-01	4.4	5.336E-02	47.60	7.482E-01	3.278E-02
45.15	7.685E-01	6.2	5.172E-02	48.13	6.957E-01	4.294E-02
46.15	7.167E-01	4.8	5.240E-02	49.18	6.500E-01	3.112E-02
46.65	9.248E-01	5.8	7.043E-02	49.70	8.395E-01	4.880E-02
47.15	1.021E 00	5.3	8.095E-02	50.23	9.277E-01	4.916E-02
47.65	6.990E-01	10.1	5.767E-02	50.75	6.357E-01	6.451E-02
48.15	9.152E-01	5.7	7.853E-02	51.28	8.331E-01	4.740E-02
49.15	4.004E-01	14.0	3.712E-02	52.33	3.652E-01	5.100E-02
50.15	7.743E-01	7.7	7.740E-02	53.37	7.075E-01	5.461E-02
50.65	6.824E-01	10.3	7.079E-02	53.90	6.241E-01	6.408E-02
52.15	4.608E-01	13.1	5.330E-02	55.47	4.227E-01	5.538E-02
55.15	3.820E-01	9.4	5.436E-02	58.60	3.525E-01	3.324E-02
56.65	4.434E-01	8.4	6.965E-02	60.16	4.105E-01	3.447E-02
58.15	3.425E-01	9.3	5.920E-02	61.72	3.181E-01	2.964E-02

SCATTERING OF 104 MEV ALPHAPARTICLES ON 56 FE

Q = -0.847 MEV I = 2+

ECM = 96.218 MEV K = 4.1465/FERMI ETA = 1.61333

LABORATORY DATA			CM DATA		
THETA DEGREE	SIGMA MB/SR	DSIGMA %	THETA DEGREE	SIGMA MB/SR	DSIGMA MB/SR
6.00	2.120E 02	37.1	6.44	1.841E 02	6.831E 01
7.00	1.520E 02	6.1	7.51	1.320E 02	8.089E 00
8.00	6.319E 01	12.2	8.59	5.490E 01	6.676E 00
8.50	2.873E 01	12.6	9.12	2.496E 01	3.146E 00
8.65	3.544E 01	11.8	9.28	3.080E 01	3.637E 00
9.00	1.255E 01	8.2	9.66	1.091E 01	8.899E-01
9.15	1.466E 01	17.0	9.82	1.274E 01	2.166E 00
9.50	8.711E 00	21.4	10.20	7.572E 00	1.618E 00
9.65	1.074E 01	3.5	10.36	9.336E 00	3.276E-01
10.00	1.797E 01	20.1	10.73	1.562E 01	3.140E 00
10.15	1.722E 01	8.4	10.89	1.497E 01	1.260E 00
10.50	3.596E 01	11.8	11.27	3.127E 01	3.705E 00
10.65	2.475E 01	9.0	11.43	2.152E 01	1.943E 00
11.00	5.717E 01	5.2	11.80	4.973E 01	2.591E 00
11.15	3.915E 01	8.7	11.97	3.406E 01	2.970E 00
11.50	7.185E 01	1.3	12.34	6.251E 01	7.842E-01
11.65	5.849E 01	5.5	12.50	5.089E 01	2.782E 00
12.00	7.532E 01	0.9	12.88	6.555E 01	5.904E-01
12.15	7.072E 01	1.7	13.04	6.155E 01	1.030E 00
12.50	7.318E 01	3.9	13.41	6.370E 01	2.490E 00
12.65	6.780E 01	1.9	13.57	5.902E 01	1.147E 00
13.00	5.911E 01	6.5	13.95	5.147E 01	3.348E 00
13.15	5.870E 01	5.0	14.11	5.112E 01	2.575E 00
13.50	4.002E 01	6.4	14.48	3.486E 01	2.234E 00
13.65	3.876E 01	9.6	14.65	3.376E 01	3.236E 00
14.00	2.727E 01	9.9	15.02	2.376E 01	2.347E 00
14.15	2.196E 01	12.7	15.18	1.913E 01	2.434E 00
14.50	1.382E 01	16.6	15.56	1.204E 01	2.004E 00
14.65	1.114E 01	30.1	15.72	9.709E 00	2.922E 00
15.00	7.446E 00	13.6	16.09	6.491E 00	8.822E-01
15.15	4.766E 00	16.4	16.25	4.155E 00	6.832E-01
15.50	2.456E 00	21.9	16.63	2.142E 00	4.686E-01
15.65	3.750E 00	17.0	16.79	3.271E 00	5.546E-01
16.00	5.101E 00	16.9	17.16	4.450E 00	7.536E-01
16.15	1.089E 01	6.8	17.32	9.501E 00	6.433E-01
16.50	9.366E 00	13.9	17.70	8.173E 00	1.138E 00
16.65	1.073E 01	6.8	17.86	9.365E 00	6.414E-01
17.00	1.582E 01	7.4	18.23	1.381E 01	1.018E 00
17.15	1.729E 01	4.3	18.39	1.510E 01	6.431E-01
17.50	2.153E 01	2.5	18.77	1.880E 01	4.631E-01
17.65	2.117E 01	2.8	18.93	1.849E 01	5.138E-01
18.00	2.377E 01	1.3	19.30	2.077E 01	2.633E-01
18.15	2.311E 01	1.8	19.46	2.019E 01	3.641E-01
18.50	2.408E 01	3.7	19.84	2.105E 01	7.800E-01
18.65	2.235E 01	1.9	20.00	1.954E 01	3.623E-01
19.00	1.979E 01	2.6	20.37	1.730E 01	4.539E-01
19.15	1.978E 01	3.8	20.53	1.730E 01	6.654E-01
19.50	1.743E 01	5.6	20.91	1.525E 01	8.546E-01
19.65	1.545E 01	6.1	21.07	1.352E 01	8.245E-01
20.00	1.266E 01	7.8	21.44	1.108E 01	8.642E-01
20.15	1.043E 01	6.1	21.60	9.128E 00	5.534E-01
20.50	7.840E 00	8.8	21.98	6.863E 00	6.032E-01
20.65	6.502E 00	7.7	22.14	5.693E 00	4.399E-01
21.00	4.500E 00	4.9	22.51	3.941E 00	1.926E-01
21.15	3.712E 00	6.6	22.67	3.251E 00	2.132E-01
21.50	3.608E 00	3.2	23.05	3.161E 00	1.008E-01
21.65	3.024E 00	4.1	23.21	2.650E 00	1.083E-01
22.00	3.628E 00	9.6	23.58	3.180E 00	3.048E-01
22.15	3.784E 00	6.3	23.74	3.318E 00	2.076E-01
22.50	5.268E 00	6.4	24.11	4.620E 00	2.960E-01
22.65	4.956E 00	6.0	24.27	4.347E 00	2.627E-01
23.00	6.806E 00	3.0	24.65	5.972E 00	1.780E-01
23.15	6.659E 00	4.3	24.81	5.844E 00	2.499E-01
23.50	7.443E 00	5.3	25.18	6.534E 00	3.473E-01
23.65	8.533E 00	3.2	25.34	7.492E 00	2.390E-01
24.00	9.241E 00	2.0	25.72	8.117E 00	1.631E-01
24.15	9.252E 00	2.2	25.88	8.127E 00	1.794E-01
24.50	9.371E 00	7.2	26.25	8.235E 00	5.890E-01
24.65	9.353E 00	1.6	26.41	8.220E 00	1.339E-01
25.00	9.049E 00	3.8	26.78	7.956E 00	3.054E-01
25.15	8.359E 00	3.0	26.94	7.351E 00	2.187E-01
25.50	7.569E 00	4.6	27.32	6.658E 00	3.062E-01
25.65	7.136E 00	3.7	27.48	6.279E 00	2.330E-01
26.00	6.040E 00	5.6	27.85	5.316E 00	3.000E-01
26.15	5.489E 00	4.8	28.01	4.832E 00	2.339E-01
26.65	3.987E 00	5.5	28.54	3.512E 00	1.925E-01
27.15	2.969E 00	4.7	29.07	2.617E 00	1.241E-01
27.65	2.301E 00	5.0	29.61	2.029E 00	1.019E-01
28.15	2.022E 00	5.1	30.14	1.784E 00	9.114E-02
28.65	2.354E 00	4.2	30.67	2.078E 00	8.778E-02
29.15	2.825E 00	3.7	31.20	2.496E 00	9.161E-02
29.65	3.308E 00	2.8	31.74	2.924E 00	8.184E-02
30.15	3.809E 00	3.1	32.27	3.369E 00	1.034E-01
30.65	3.787E 00	3.8	32.80	3.352E 00	1.260E-01
31.15	3.718E 00	2.5	33.33	3.293E 00	8.210E-02
31.37	3.350E 00	4.1	33.57	2.968E 00	1.212E-01
31.65	3.788E 00	4.6	33.86	3.357E 00	1.547E-01
32.15	2.724E 00	7.0	34.39	2.416E 00	1.700E-01
32.65	2.263E 00	3.9	34.93	2.008E 00	7.891E-02
32.87	2.127E 00	4.3	35.16	1.888E 00	8.169E-02
33.15	1.624E 00	5.6	35.46	1.442E 00	8.022E-02
33.65	1.761E 00	5.1	35.99	1.565E 00	8.047E-02
34.15	1.318E 00	3.5	36.52	1.172E 00	4.074E-02
34.37	1.330E 00	3.8	36.75	1.183E 00	4.450E-02
34.65	1.360E 00	7.2	37.05	1.210E 00	8.751E-02
35.15	1.278E 00	4.3	37.58	1.138E 00	4.883E-02
35.65	1.388E 00	3.2	38.11	1.237E 00	3.914E-02
35.87	1.376E 00	4.0	38.34	1.227E 00	4.912E-02
36.15	1.657E 00	4.7	38.64	1.478E 00	6.981E-02
36.65	1.667E 00	4.9	39.17	1.488E 00	7.266E-02
37.15	1.685E 00	3.0	39.70	1.505E 00	4.496E-02
37.65	1.622E 00	5.1	40.23	1.450E 00	7.329E-02
38.15	1.570E 00	5.1	40.76	1.404E 00	7.205E-02
38.65	1.329E 00	3.4	41.28	1.190E 00	4.074E-02
39.15	1.344E 00	5.5	41.81	1.204E 00	6.665E-02
39.65	1.050E 00	13.2	42.34	9.414E-01	1.246E-01
40.15	5.716E-01	6.1	42.87	5.129E-01	3.138E-02
40.65	1.062E 00	10.5	43.40	9.537E-01	9.968E-02
41.15	1.015E 00	6.0	43.93	9.122E-01	5.431E-02
41.65	8.359E-01	3.7	44.45	7.519E-01	2.802E-02
42.15	1.158E 00	5.6	44.98	1.042E 00	5.869E-02
42.65	1.092E 00	6.3	45.51	9.839E-01	6.155E-02
43.15	8.967E-01	3.6	46.03	8.086E-01	2.913E-02
44.15	1.024E 00	5.9	47.09	9.250E-01	5.481E-02
44.65	8.734E-01	4.2	47.61	7.897E-01	3.325E-02
45.15	8.667E-01	6.0	48.14	7.843E-01	4.674E-02
46.15	7.330E-01	4.4	49.19	6.645E-01	2.905E-02
46.65	8.028E-01	6.2	49.72	7.285E-01	4.551E-02
47.15	7.786E-01	6.1	50.24	7.071E-01	4.329E-02
47.65	6.674E-01	8.7	50.77	6.067E-01	5.297E-02
48.15	6.821E-01	6.6	51.29	6.207E-01	4.076E-02
49.15	5.710E-01	9.9	52.34	5.205E-01	5.169E-02
50.15	6.071E-01	8.3	53.39	5.545E-01	4.611E-02
50.65	5.755E-01	11.3	53.91	5.262E-01	5.921E-02
52.15	3.418E-01	15.4	55.48	3.134E-01	4.838E-02
52.65	3.870E-01	8.2	56.00	3.552E-01	2.922E-02
54.15	1.654E-01	12.8	57.57	1.523E-01	1.945E-02
55.15	3.736E-01	9.0	58.61	3.447E-01	3.110E-02
56.65	2.937E-01	10.3	60.17	2.718E-01	2.808E-02
58.15	3.223E-01	9.5	61.73	2.992E-01	2.829E-02
63.15	1.187E-01	14.4	66.91	1.114E-01	1.604E-02
64.65	8.609E-02	17.5	68.46	8.109E-02	1.419E-02
66.15	6.716E-02	19.0	70.01	6.348E-02	1.206E-02

SCATTERING OF 104 MEV ALPHAPARTICLES ON 56 FE

Q = -2.085 MEV   I = 4+

ECM = 94.979 MEV   K = 4.1198/FERMI   ETA = 1.62381

LABORATORY DATA THETA DEGREE	SIGMA MB/SR	DSIGMA %	CM DATA THETA DEGREE	SIGMA MB/SR	DSIGMA MB/SR
12.15	8.811E-01	11.4	13.04	7.662E-01	8.757E-02
12.65	7.182E-01	7.5	13.58	6.247E-01	4.686E-02
13.15	8.691E-01	9.3	14.12	7.562E-01	7.030E-02
13.65	6.362E-01	9.2	14.65	5.537E-01	5.067E-02
14.15	7.940E-01	11.5	15.19	6.912E-01	7.948E-02
14.65	1.029E 00	9.4	15.72	8.961E-01	8.409E-02
15.15	7.936E-01	13.5	16.26	6.913E-01	9.330E-02
16.15	1.085E 00	12.9	17.33	9.458E-01	1.219E-01
16.65	1.097E 00	12.8	17.87	9.566E-01	1.229E-01
17.15	2.726E-01	21.0	18.40	2.378E-01	4.999E-02
17.65	2.186E-01	14.9	18.94	1.908E-01	2.842E-02
18.15	2.841E-01	14.1	19.47	2.480E-01	3.489E-02
19.65	3.981E-01	12.5	21.08	3.480E-01	4.336E-02
20.15	4.808E-01	10.0	21.61	4.204E-01	4.213E-02
20.65	6.430E-01	8.3	22.15	5.625E-01	4.665E-02
21.15	6.065E-01	9.1	22.68	5.308E-01	4.841E-02
21.65	5.154E-01	10.1	23.22	4.513E-01	4.543E-02
22.15	4.549E-01	11.3	23.75	3.985E-01	4.487E-02
22.65	3.234E-01	13.7	24.28	2.834E-01	3.891E-02
23.15	2.617E-01	13.7	24.82	2.295E-01	3.134E-02
23.65	2.659E-01	11.9	25.35	2.333E-01	2.771E-02
24.15	2.826E-01	10.4	25.89	2.481E-01	2.579E-02
24.65	2.751E-01	8.2	26.42	2.416E-01	1.974E-02
25.15	3.217E-01	10.6	26.95	2.827E-01	2.994E-02
25.65	3.715E-01	10.3	27.49	3.266E-01	3.379E-02
26.15	4.324E-01	11.5	28.02	3.804E-01	4.367E-02
26.65	4.582E-01	9.3	28.55	4.033E-01	3.765E-02
27.15	4.765E-01	7.0	29.09	4.196E-01	2.921E-02
27.65	4.304E-01	11.5	29.62	3.792E-01	4.370E-02
28.15	3.971E-01	9.0	30.15	3.501E-01	3.143E-02
28.65	3.727E-01	8.3	30.69	3.288E-01	2.719E-02
29.15	3.147E-01	7.9	31.22	2.778E-01	2.201E-02
29.65	2.688E-01	8.3	31.75	2.374E-01	1.979E-02
30.15	2.842E-01	10.9	32.28	2.512E-01	2.731E-02
30.65	2.273E-01	15.5	32.81	2.010E-01	3.111E-02
31.15	2.358E-01	10.1	33.35	2.087E-01	2.110E-02
31.37	2.196E-01	9.0	33.58	1.944E-01	1.752E-02
31.65	2.844E-01	13.8	33.88	2.518E-01	3.473E-02
32.15	1.697E-01	15.8	34.41	1.504E-01	2.378E-02
32.65	2.619E-01	8.5	34.94	2.322E-01	1.981E-02
32.87	2.597E-01	7.3	35.17	2.303E-01	1.680E-02
33.15	3.351E-01	10.7	35.47	2.973E-01	3.182E-02
33.65	3.596E-01	11.3	36.00	3.193E-01	3.614E-02
34.15	2.436E-01	7.8	36.53	2.165E-01	1.685E-02
34.37	2.194E-01	9.5	36.77	1.950E-01	1.849E-02
34.65	2.474E-01	13.3	37.06	2.200E-01	2.936E-02
35.15	2.199E-01	13.5	37.59	1.957E-01	2.641E-02
35.65	1.519E-01	10.1	38.12	1.353E-01	1.370E-02
35.87	1.390E-01	11.9	38.36	1.238E-01	1.470E-02
36.15	1.123E-01	18.6	38.65	1.001E-01	1.858E-02
36.65	2.072E-01	13.8	39.18	1.848E-01	2.549E-02
37.15	1.309E-01	11.6	39.71	1.168E-01	1.359E-02
37.65	9.357E-02	20.6	40.24	8.357E-02	1.720E-02
38.15	1.173E-01	17.8	40.77	1.048E-01	1.866E-02
38.65	1.267E-01	10.6	41.30	1.133E-01	1.197E-02
39.15	1.499E-01	16.0	41.83	1.342E-01	2.146E-02
39.65	1.991E-01	14.0	42.36	1.784E-01	2.499E-02
40.15	1.199E-01	10.4	42.89	1.075E-01	1.122E-02
40.65	1.564E-01	15.8	43.41	1.404E-01	2.219E-02
41.15	1.457E-01	15.7	43.94	1.309E-01	2.055E-02
41.65	1.064E-01	10.7	44.47	9.565E-02	1.019E-02
42.15	1.114E-01	18.1	45.00	1.002E-01	1.809E-02
42.65	1.168E-01	18.3	45.53	1.052E-01	1.924E-02
43.15	8.493E-01	1.2	46.05	7.654E-01	9.283E-03
44.15	1.079E-01	18.3	47.11	9.741E-02	1.780E-02
44.65	7.816E-02	15.0	47.63	7.062E-02	1.062E-02
45.15	9.411E-02	17.7	48.16	8.511E-02	1.507E-02
46.15	6.163E-02	15.5	49.21	5.584E-02	8.633E-03
46.65	9.055E-02	18.8	49.74	8.212E-02	1.544E-02
47.15	1.023E-01	17.0	50.26	9.286E-02	1.578E-02
47.65	7.296E-02	26.3	50.79	6.629E-02	1.743E-02
48.15	1.354E-02	46.4	51.31	1.231E-02	5.716E-03
49.15	4.327E-02	35.7	52.36	3.942E-02	1.449E-02
50.15	1.610E-01	13.5	53.41	1.470E-01	1.991E-02
50.65	7.643E-02	30.7	53.93	6.984E-02	2.143E-02
51.15	1.653E-02	48.4	54.46	1.512E-02	7.319E-03
52.15	3.748E-02	45.1	55.50	3.435E-02	1.550E-02
52.65	8.389E-02	17.6	56.02	7.696E-02	1.355E-02
54.15	1.735E-02	39.0	57.59	1.597E-02	6.230E-03
55.15	1.029E-01	16.9	58.63	9.489E-02	1.599E-02
56.65	5.619E-02	23.8	60.19	5.198E-02	1.236E-02
58.15	5.179E-02	23.6	61.75	4.806E-02	1.134E-02
63.15	1.172E-02	45.2	66.94	1.100E-02	4.967E-03
64.65	3.600E-02	26.9	68.48	3.390E-02	9.115E-03
66.15	7.950E-03	59.7	70.03	7.512E-03	4.487E-03

SCATTERING OF 104 MEV ALPHAPARTICLES ON 56 FE

Q = -2.658 MEV I = 2+

ECM = 94.406 MEV K = 4.1073/FERMI ETA = 1.62873

LABORATORY DATA THETA DEGREE	SIGMA MB/SR	DSIGMA %	CM DATA THETA DEGREE	SIGMA MB/SR	DSIGMA MB/SR
8.65	4.779E 00	10.7	9.29	4.148E 00	4.434E-01
9.15	2.397E 00	13.5	9.83	2.081E 00	2.806E-01
9.65	1.822E 00	6.3	10.36	1.582E 00	9.993E-02
10.15	2.560E 00	7.0	10.90	2.223E 00	1.562E-01
10.65	2.936E 00	6.8	11.44	2.550E 00	1.736E-01
11.15	3.885E 00	6.8	11.97	3.375E 00	2.306E-01
11.65	4.992E 00	4.4	12.51	4.338E 00	1.907E-01
12.15	5.516E 00	3.8	13.05	4.795E 00	1.809E-01
12.65	4.729E 00	4.9	13.58	4.112E 00	2.034E-01
13.15	3.675E 00	7.0	14.12	3.196E 00	2.247E-01
13.65	2.744E 00	9.5	14.65	2.387E 00	2.258E-01
14.15	1.590E 00	12.3	15.19	1.384E 00	1.703E-01
14.65	1.163E 00	12.1	15.73	1.012E 00	1.221E-01
15.15	5.603E-01	19.5	16.26	4.879E-01	9.500E-02
15.65	5.433E-01	17.1	16.80	4.733E-01	8.106E-02
16.15	1.338E 00	6.9	17.33	1.166E 00	8.059E-02
16.65	5.802E-01	16.0	17.87	5.058E-01	8.109E-02
17.15	1.289E 00	9.9	18.41	1.124E 00	1.114E-01
17.65	1.577E 00	8.9	18.94	1.376E 00	1.221E-01
18.15	2.389E 00	4.9	19.48	2.085E 00	1.027E-01
18.65	2.077E 00	4.7	20.01	1.813E 00	8.470E-02
19.15	1.904E 00	6.0	20.55	1.663E 00	1.005E-01
19.65	1.499E 00	7.7	21.08	1.310E 00	1.007E-01
20.15	1.021E 00	9.4	21.62	8.925E-01	8.350E-02
20.65	7.668E-01	11.5	22.15	6.706E-01	7.717E-02
21.15	3.802E-01	13.1	22.69	3.326E-01	4.359E-02
22.15	6.401E-01	8.8	23.75	5.605E-01	4.934E-02
22.65	5.037E-01	10.1	24.29	4.413E-01	4.442E-02
23.15	5.544E-01	9.5	24.82	4.860E-01	4.595E-02
23.65	5.098E-01	6.6	25.36	4.471E-01	2.970E-02
24.15	7.248E-01	5.5	25.89	6.360E-01	3.517E-02
24.65	6.871E-01	6.3	26.43	6.032E-01	3.789E-02
25.15	4.721E-01	7.1	26.96	4.147E-01	2.930E-02
25.65	5.345E-01	5.2	27.49	4.697E-01	2.465E-02
26.15	4.022E-01	7.6	28.03	3.537E-01	2.695E-02
26.65	3.386E-01	9.4	28.56	2.979E-01	2.799E-02
27.15	2.607E-01	10.6	29.09	2.295E-01	2.442E-02
27.65	1.652E-01	13.3	29.63	1.455E-01	1.940E-02
28.15	9.484E-02	16.2	30.16	8.359E-02	1.355E-02
28.65	1.756E-01	10.6	30.69	1.549E-01	1.635E-02
29.15	1.366E-01	12.6	31.22	1.205E-01	1.519E-02
29.65	2.407E-01	9.8	31.76	2.125E-01	2.078E-02
31.15	2.628E-01	8.6	33.35	2.325E-01	2.009E-02
31.37	2.666E-01	8.2	33.59	2.359E-01	1.929E-02
32.65	2.472E-01	8.9	34.95	2.191E-01	1.955E-02
32.87	2.220E-01	9.1	35.18	1.968E-01	1.792E-02
34.15	1.099E-01	13.1	36.54	9.762E-02	1.276E-02
34.37	1.229E-01	12.4	36.77	1.092E-01	1.359E-02
35.65	1.379E-01	11.8	38.13	1.228E-01	1.446E-02
35.87	1.166E-01	13.1	38.36	1.038E-01	1.359E-02
37.15	1.385E-01	11.9	39.72	1.236E-01	1.468E-02
38.65	9.702E-02	13.8	41.31	8.676E-02	1.200E-02
40.15	6.802E-02	16.6	42.89	6.097E-02	1.013E-02
41.65	6.375E-02	14.1	44.48	5.729E-02	8.066E-03
43.15	5.264E-02	19.3	46.06	4.743E-02	9.136E-03
44.65	6.028E-02	17.3	47.64	5.445E-02	9.404E-03
46.15	3.650E-02	16.4	49.22	3.306E-02	5.427E-03
47.65	2.991E-02	41.0	50.80	2.717E-02	1.114E-02
49.15	4.264E-02	36.0	52.37	3.884E-02	1.399E-02
50.65	4.568E-02	39.7	53.94	4.173E-02	1.655E-02
52.15	3.726E-02	44.7	55.51	3.414E-02	1.527E-02

SCATTERING OF 104 MEV ALPHAPARTICLES ON 56 FE

Q = -4.505 MEV I = 3-

ECM = 92.559 MEV K = 4.0669/FERMI ETA = 1.64491

LABORATORY DATA			CM DATA		
THETA DEGREE	SIGMA MB/SR	DSIGMA %	THETA DEGREE	SIGMA MB/SR	DSIGMA MB/SR
8.65	3.949E 01	18.5	9.30	3.423E 01	6.319E 00
9.15	3.132E 01	11.4	9.83	2.715E 01	3.104E 00
9.65	3.710E 01	5.1	10.37	3.217E 01	1.648E 00
10.15	2.207E 01	2.5	10.91	1.914E 01	4.753E-01
10.65	1.315E 01	11.2	11.44	1.141E 01	1.276E 00
11.15	7.698E 00	8.0	11.98	6.679E 00	5.373E-01
11.65	5.863E 00	4.2	12.52	5.089E 00	2.150E-01
12.15	5.822E 00	4.7	13.05	5.054E 00	2.373E-01
12.65	7.615E 00	6.9	13.59	6.613E 00	4.552E-01
13.15	1.074E 01	5.6	14.13	9.329E 00	5.264E-01
13.65	1.298E 01	3.3	14.66	1.128E 01	3.672E-01
14.15	1.337E 01	3.0	15.20	1.162E 01	3.451E-01
14.65	1.516E 01	2.2	15.74	1.318E 01	2.939E-01
15.15	1.395E 01	3.9	16.27	1.213E 01	4.715E-01
15.65	1.211E 01	4.9	16.81	1.054E 01	5.137E-01
16.15	8.799E 00	5.9	17.35	7.658E 00	5.265E-01
16.65	6.690E 00	7.6	17.88	5.824E 00	4.410E-01
17.15	4.837E 00	8.7	18.42	4.213E 00	3.654E-01
17.65	2.789E 00	9.4	18.95	2.430E 00	2.272E-01
18.15	2.495E 00	4.4	19.49	2.175E 00	9.622E-02
18.65	2.608E 00	4.8	20.02	2.274E 00	1.100E-01
19.15	3.341E 00	5.8	20.56	2.914E 00	1.680E-01
19.65	4.012E 00	5.1	21.10	3.501E 00	1.785E-01
20.15	4.964E 00	3.8	21.63	4.334E 00	1.666E-01
20.65	5.359E 00	3.0	22.17	4.681E 00	1.401E-01
21.15	5.024E 00	3.2	22.70	4.390E 00	1.392E-01
21.65	5.000E 00	4.8	23.24	4.371E 00	2.109E-01
22.15	3.174E 00	8.6	23.77	2.776E 00	2.379E-01
22.65	2.588E 00	6.7	24.31	2.265E 00	1.510E-01
23.15	1.871E 00	5.8	24.84	1.638E 00	9.420E-02
23.65	2.108E 00	3.0	25.37	1.846E 00	5.544E-02
24.15	1.655E 00	5.4	25.91	1.450E 00	7.800E-02
24.65	1.402E 00	3.6	26.44	1.229E 00	4.398E-02
25.15	1.615E 00	4.3	26.98	1.417E 00	6.060E-02
25.65	1.799E 00	3.0	27.51	1.579E 00	4.744E-02
26.15	1.825E 00	3.0	28.04	1.603E 00	4.882E-02
26.65	2.038E 00	3.8	28.58	1.791E 00	6.799E-02
27.15	2.156E 00	2.9	29.11	1.896E 00	5.480E-02
27.65	2.012E 00	4.2	29.64	1.770E 00	7.352E-02
28.15	1.577E 00	7.8	30.18	1.388E 00	1.084E-01
28.65	9.508E-01	10.5	30.71	8.375E-01	8.765E-02
29.15	6.742E-01	5.3	31.24	5.942E-01	3.132E-02
29.65	9.824E-01	4.9	31.78	8.664E-01	4.261E-02
31.15	7.825E-01	5.4	33.37	6.914E-01	3.753E-02
31.37	7.388E-01	5.0	33.61	6.530E-01	3.243E-02
32.65	8.538E-01	4.7	34.97	7.560E-01	3.551E-02
32.87	8.717E-01	4.0	35.20	7.721E-01	3.073E-02
34.15	7.807E-01	4.9	36.56	6.927E-01	3.415E-02
34.37	7.722E-01	5.0	36.80	6.854E-01	3.435E-02
35.65	5.552E-01	6.0	38.15	4.937E-01	2.986E-02
35.87	5.408E-01	6.1	38.39	4.811E-01	2.927E-02
37.15	3.996E-01	7.2	39.75	3.561E-01	2.561E-02
38.65	3.627E-01	7.1	41.33	3.240E-01	2.300E-02
40.15	3.012E-01	7.9	42.92	2.697E-01	2.136E-02
41.65	2.735E-01	8.1	44.51	2.455E-01	2.000E-02
43.15	2.111E-01	9.9	46.09	1.900E-01	1.884E-02
46.15	1.843E-01	8.7	49.25	1.668E-01	1.448E-02
47.65	2.331E-01	14.8	50.83	2.115E-01	3.122E-02
49.15	1.885E-01	17.2	52.40	1.716E-01	2.950E-02
50.65	1.444E-01	22.7	53.97	1.318E-01	2.986E-02
52.15	1.480E-01	23.2	55.54	1.355E-01	3.141E-02